Accepted Manuscript

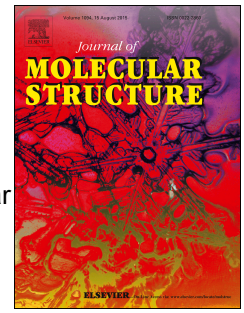

An analysis of structural and spectroscopic signatures, the reactivity study of synthetized 4,6-dichloro-2-(methylsulfonyl)pyrimidine: A potential third-order nonlinear optical material

P. Krishna Murthy, Clodoaldo Valverde, V. Suneetha, Stevan Armaković, Sanja J. Armaković, N. Usha Rani, N. Venkatasubba Naidu

PII: S0022-2860(19)30282-0

DOI: https://doi.org/10.1016/j.molstruc.2019.03.021

Reference: MOLSTR 26290

To appear in: *Journal of Molecular Structure*

Received Date: 1 September 2018

Revised Date: 19 February 2019

Accepted Date: 6 March 2019

Please cite this article as: P.K. Murthy, C. Valverde, V. Suneetha, S. Armaković, S.J. Armaković, N.U. Rani, N.V. Naidu, An analysis of structural and spectroscopic signatures, the reactivity study of synthetized 4,6-dichloro-2-(methylsulfonyl)pyrimidine: A potential third-order nonlinear optical material, *Journal of Molecular Structure* (2019), doi: https://doi.org/10.1016/j.molstruc.2019.03.021.

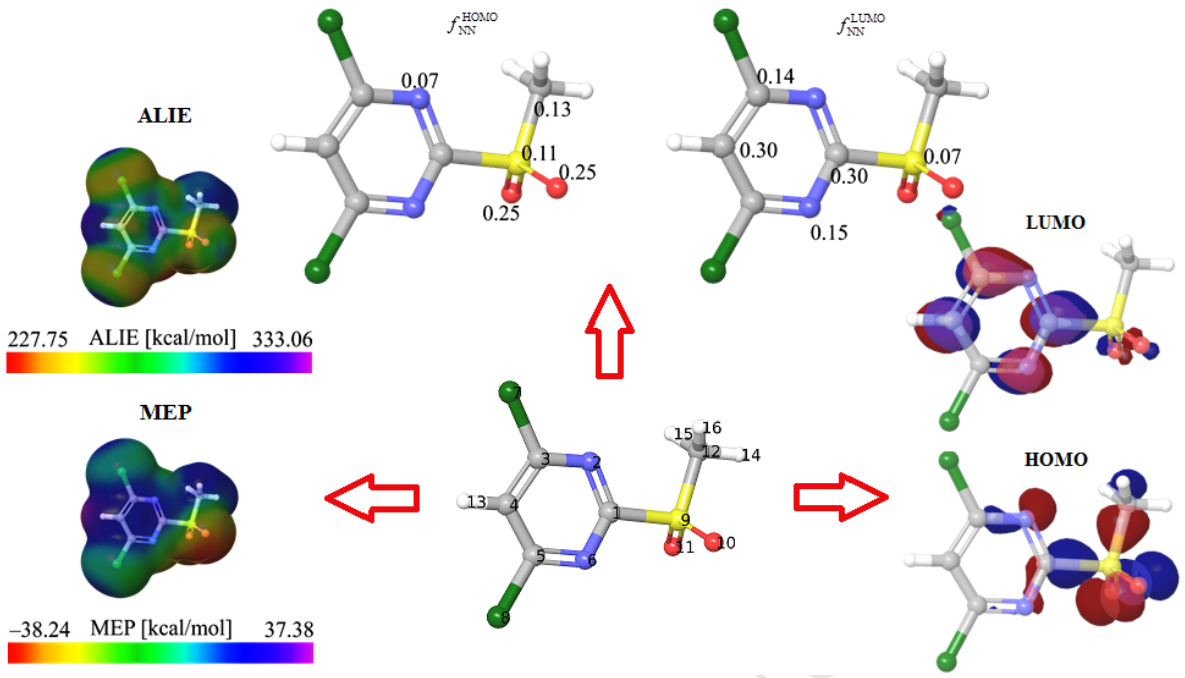

An analysis of structural and spectroscopic signatures, the reactivity study of synthetized 4,6-dichloro-2-(methylsulfonyl)pyrimidine: A potential third-order nonlinear optical material

P. Krishna Murthy[a*], Clodoaldo Valverde[b,c], V. Suneetha[a,d], Stevan Armaković[e], Sanja J. Armaković[f], N. Usha Rani[g], N. Venkatasubba Naidu[h]

[a]Department of Chemistry, Bapatla Engineering College (Autonomous), Acharya Nagarjuna University Post Graduate Research Centre, Bapatla-522 102, A.P., India.

[b]Laboratório de Modelagem Molecular Aplicada e Simulação (LaMMAS), Campus de Ciências Exatas e Tecnológicas, Universidade Estadual de Goiás, 75001-970, Anápolis, GO, Brazil.

[c]Universidade Paulista, 74845-090, Goiânia, GO, Brazil; Centro Universitário de Anápolis, 75083-515, Anápolis, GO, Brazil.

[d]Department of Chemistry, Bapatla College of Arts and Sciences, Baptla-522 101, A.P., India.

[e]University of Novi Sad, Faculty of Sciences, Department of Physics, Trg D. Obradovića 4, 21000 Novi Sad, Serbia.

[f]University of Novi Sad, Faculty of Sciences, Department of Chemistry, Biochemistry and Environmental Protection, Trg D. Obradovića 3, 21000 Novi Sad, Serbia.

[g]Department of Freshman Engineering, P.V.P. Siddhartha Institute of Technology, Vijayawada-520 007.

[h]Department of Chemistry, Sri Venkateswara University, Tirupati -517 512, A.P., India.

*Corresponding author: krishnamurthypotla@gmail.com

Abstract

In this work the 4,6-dichloro-2-(methylsulfonyl)pyrimidine (DCMSP) has been synthesized from 4,6-dichloro-2-(methylthio)pyrimidine, its molecular and electronic structure was authenticated by detailed spectroscopic signature studies (*via* SCXRD, FT-Raman, FT-IR and (^{1}H & ^{13}C) NMR), Hirshfeld surface analysis and DFT calculations. The solid-state crystal structure of DCMSP corroborated by the single crystal X-ray diffraction studies, features C-H$\cdots$O and $\pi\cdots\pi$ interactions. Quantum chemical calculations of DCMSP have been performed at DFT/B3LYP/6-311++G(d,p) level of theory. The detailed assignment of each the vibrational mode was done on the basis of potential energy distribution (PED) by using the VEDA4 program and these results have been correlated with the experimental data. We calculated the linear and nonlinear optical properties of the title compound to understand the

linear and nonlinear optical behavior in both static and dynamic fields using an iterative electrostatic embedding scheme and density functional theory (DFT) methods with standard and long-range corrected functionals. We also performed a study of the linear refractive index and nonlinear optical susceptibility $\chi^{(3)}$ of the crystal as a function of frequency. An estimate of linear and nonlinear macroscopic quantities confirms their suitability for nonlinear optical devices such as optical limiting and optical switching. Investigation of local and global reactivity parameters of DCMSP was carried out by the calculation of molecular electrostatic potential (MEP), average local ionization energies (ALIE) surfaces and atomic Fukui indices in the gas phase. Stability in water and sensitivity towards autoxidation process has been investigated by radial distribution function (RDF) and bond dissociation energies (BDE) calculation after molecular dynamic simulations.

Keywords: Pyrimidine; NLO properties; ALIE; BDE; RDF; Fukui functions.

1. Introduction

Historically, inorganic crystals are main materials applied for nonlinear optical field with current applications [1-3], but the last few years, the use of organic crystals as non-linear optical (NLO) materials has been growing motivated by to the easy manipulation of these crystals, which allow control the material NLO properties [4]. Studies of non-linear optical processes contribute significantly to the development of photonics [5, 6], spectroscopy [7, 8], fiber optic lines [7], optical switches [9], frequency converters [1], electro-optic modulators [10], and still with thermal application [11]. Third-order nonlinear materials with inefficient nonlinear absorption and strong nonlinear refraction have received considerable attention from researchers because of their potential uses in optical signal processing devices [12,13]. Organic crystals with good third-order nonlinear optical properties have attracted attention because such compounds were possessing good trade-off between optical transparency and optical power limiting performance [12–17].

Computational molecular modeling techniques have become indispensable tools for studying fundamental reactive properties of various molecular structures [18-23]. The ab-initio calculations have proven to be especially useful for the understanding of the local reactivity of molecules. In this work, we endeavor synthesis, spectroscopic investigations (*via* SCXRD, FT-Raman, FT-IR and (^{1}H &^{13}C) NMR), and Hirshfeld surface analysis of 4,6-dichloro-2-(methylsulfonyl)pyrimidine (DCMSP). We apply ab-initio methods in conjunction with a supermolecule approach which includes the Møller-Plesset Perturbation Theory (MP2) and the Density Functional Theory (DFT) at the CAM-B3LYP level to determine the linear

refractive index and the third-order nonlinear susceptibility of the crystal (DCMSP). The local reactivity properties of DCMSP molecule have been investigated by calculating the molecular electrostatic potential (MEP), average local ionization energy (ALIE), atomic Fukui indices, bond dissociation energies (BDE) and bond dissociation energies for hydrogen abstraction (H-BDE). The influence of water and identification of DCMSP's atoms with pronounced interactions with water molecules have been assessed by molecular dynamics (MD) simulations and radial distribution functions (RDF).

2. Methodology

2.1. General remarks

All chemicals and reagents were purchased from a commercial source and used as such without further purification. The synthesis was performed under anaerobic conditions. The Fourier transform infra spectrum was recorded using the KBr disc on ATR module ALPHA-T Bruker FT-IR spectrometer in the range 4000-400 cm^{-1} with resolution ±2cm^{-1} (Figure 1). The Fourier transform Raman spectrum was recorded on Bruker RFS 100/s, Germany (laser source: Nd:YAG, excitation wavelength: 1064 nm, spectral resolution ± 2cm^{-1}) for the solid sample in the range 50-4000 cm^{-1} (Figure 2). ^{1}H and ^{13}C-NMR chemical shift values measured in ppm on Bruker 400 MHz FT-NMR spectrometer using TMS as internal standard and the sample was dissolved in a DMSO-d_6 solvent.

2.2. Synthesis of 4,6-dichloro-2-(methylsulfonyl)pyrimidine

4,6-dichloro-2-(methylthio)pyrimidine (0.7g, 3.608 mmol) was dissolved in dichloromethane (15 mL), cooled to $0^{o}C$ and meta-Chloroperoxybenzoic acid (m-CPBA) was added (1.55g, 9.011 mmol) portion wise to the reaction mixture at the same temperature. After addition, the reaction mixture was allowed to stir for 4 hours at room temperature. Then the reaction mass was quenched with an aqueous solution of sodium thiosulphate (11 mL) and extracted with dichloromethane (2 x 10 mL). Combined organic layer was washed with saturated aqueous $NaHCO_3$ solution (15 mL), brine solution (7 mL), dried over anhydrous $MgSO_4$, filtered and the filtrate was evaporated under reduced pressure to afford 4,6-dichloro-2-(methylsulfonyl)pyrimidine (0.65 g, 80.20%) as off-white solid (Scheme -1).

2.3. X-ray crystallography

A suitable block shape crystal with dimension 0.12×0.16×0.18 mm was selected and mounted on a Bruker Smart APEX-II diffractometer using graphite monochromated MoKα (λ = 0.71073 Å) radiation and detector (CCD). The crystal was kept at 296 K during data collection. The structure was solved using SHELXS-97 [24] structure solution program then refined with the ShelXL [24] refinement package using Least Squares minimization. All the

geometrical calculations were carried out using the program PLATON [25] associated the WinGX suite [26]. The molecular and packing diagrams in solid state were generated using the software MERCURY [27].

2.4. Computational details

Ab-initio and DFT calculations on DCMSP have been performed with the Gaussian 09W computational package [28] and Schrödinger Materials Science Suite 2018-1 [29]. The starting molecular geometry of DCMSP was taken from experimental X-ray crystal structure. The full geometry optimization, analytic harmonic frequency calculations, HOMO-LUMO energies (FMO orbitals), global reactivity parameters, NBO analysis, Mullikan charges and molecular electrostatic potential (MEP) were carried out by the DFT approach with B3LYP (Becke three-parameter Lee-Yang-Parr) functional [30] using 6-311++G(d,p) basis set. The assignment of each vibrational frequency was done by PED analysis using VEDA4 program [31]. The calculated wavenumbers were scaled by a scaling factor 0.9613 for better agreement with experimental values [32]. Chemical shift values were computed by GIAO (Gauge-Independent Atomic Orbital) method [33] and electronic spectra were calculated by the TD-DFT method [34].

In order to study the linear and nonlinear optical (NLO) properties of the DCMSP crystal, we used the supermolecule (SM) approach to simulate the polarization of the crystalline environment in a single DCMSP molecule. This approach consists of building a bulk formed by a set of unit cells arranged in a 13×13×13 configuration. Each unit cell has 4 molecules and each molecule has 16 atoms, thus creating a bulk with 140,576 atoms, as shown in Figure S1. We will call this bulk *an embedded molecule or crystal DCMSP*. This isolated molecule has a blue highlight in the centre of the bulk. The atoms that are around the structure in blue were considered as punctual charges. Thus, the effects of intermolecular interactions make it possible to estimate the values of crystal properties, taking as a starting point the results obtained from the isolated molecule DCMSP.

The iterative process of the SM approach is performed in several steps: step 0, the partial atomic charge of the atoms of the isolated molecule is determined, via a ChelpG fit, by the MP2 method using the 6-311++G(d,p) basis set; then each atom of the bulk is replaced by its partial atomic charge previously obtained via fit Chelpg. At this moment, the static electric properties are calculated, dipole moment (μ), linear polarizability (α) and second hyperpolarizability (γ). In step 1, the partial atomic charges of the atoms of the isolated molecule are determined again and then we replace the value of these atomic charges in each atom of the bulk and then the electrical properties are again calculated. This iterative process

continues until the convergence of the electric dipole moment is obtained, which is treated as the electrostatic equilibrium between the isolated and neighbouring molecules [35], see Figure S2.

In each iterative process, the linear and non-linear electrical properties were calculated for both the static and dynamic cases of the embedded molecule. In the calculations of dipole moment and linear polarizability, we used the MP2 method and for the calculation of the second hyperpolarizability, we used the Density Functional Theory (CAM-B3LYP) method; in both cases, we used the 6-311++G(d,p) basis set. This choice was due to the satisfactory results obtained previously for similar systems, as demonstrated in [36].

Fonseca et al. [37] used the SM approach for the calculation of the dipole moment and the first hyper-polarizability and those results compared with experimental values, show mutual agreement. In another study, Santos et al. [38] used the SM approach for the calculation of linear $\chi^{(1)}$ and nonlinear second-order $\chi^{(2)}$ susceptibilities of urea and thiourea, theoretical results were very close to the experiment's reports. A recent literature shows [36] the SM approach was successfully used to calculate $\chi^{(1)}$, $\chi^{(2)}$ for 3-methyl-4-nitropyridine-1-oxide molecule and again the results are good in agreement with the experimental reports. In recent years, the SM approach has been successfully applied in several studies [39-49].

The electrical parameters of the crystal DCMSP were calculated using the following expressions, the total dipole moment,

$$\mu = \left(\mu_x^2 + \mu_y^2 + \mu_z^2\right)^{1/2}, \tag{1}$$

the average of the linear polarizability,

$$\bar{\alpha} = \frac{1}{3}\left(\alpha_{xx} + \alpha_{yy} + \alpha_{zz}\right), \tag{2}$$

and the average of the second hyperpolarizability, in Kleinmann's [50] symmetry,

$$\bar{\gamma} = \frac{1}{5}\left[\gamma_{xxxx} + \gamma_{yyyy} + \gamma_{zzzz} + 2\left(\gamma_{xxyy} + \gamma_{xxzz} + \gamma_{yyzz}\right)\right]. \tag{3}$$

The average linear polarizability and the average second hyperpolarizability can be related with the linear refractive index (n_o) of the crystal by the Clausius-Mossotti relation, and with the third-order electric susceptibility ($\chi^{(3)}$), through the expressions,

$$\frac{n_o^2 - 1}{n_o^2 + 2} = \frac{4\pi N}{3}\langle\alpha\rangle, \tag{4}$$

and

$$\chi^{(3)} = \frac{f^4 N\bar{\gamma}}{\epsilon_o V}, \tag{5}$$

where N is the number of molecules (Z) per unit cell volume (V) and f is the Lorentz local field correction factor given by,

$$f = \frac{(n_o^2 + 2)}{3}. \quad (6)$$

DFT calculations and molecular dynamics (MD) simulations were also performed by Jaguar [51-53] and Desmond [53-56] programs, respectively. Input files and the visualization of results have been achieved by Maestro GUI [57]. Jaguar, Desmond and Maestro programs were used as incorporated in Schrödinger Materials Science Suite 2018-1 [29]. For DFT calculations, a B3LYP exchange-correlation functional was used. Calculations of MEP, ALIE and atomic Fukui indices were done with 6-311++G(d,p) basis set. BDE and H-BDE values have been obtained with 6-311G(d,p) basis set. MD simulation was performed with OPLS3 [54, 58-60], together with simulation time set to 10 ns, while the cut off radius was set to 12 Å. The temperature was set to 300 K and the pressure to 1.0325 bar. The MD system was modeled as one DCMSP molecule surrounded by ~2500 water molecules, all placed in a cubic box. The system was considered as an NPT ensemble type. The solvent was described by a simple point charge (SPC) model [61].

3. Results & analysis

3.1. Crystal structure description

The title compound DCMSP ($C_5H_4Cl_2N_2O_2S$), crystallizes in a triclinic $P\bar{1}$ space group with two symmetrically independent molecules in the asymmetric unit. The crystallographic data and refinement parameters are listed DCMSP are listed in Table 1 and geometric parameters for hydrogen bonding and other intermolecular contacts (Å, ^{o}) operating in the crystal structure of DCMSP in Table 2. The crystal structure description of DCMSP was included in supplementary information.

3.2. Hirshfeld surface analysis

3D-Hirshfeld surfaces [62-64] associated 2D-finger print analysis [65-67] was performed using a powerful graphical tool CrystalExplorer3.1 suite [68], which accept CIF as the input file. The 3D-Hirshfeld surfaces and 2D-finger print plots of present investigated compound depicted in Figure 3. The surfaces title compound have been mapped over d_{norm}(1), *shape index* (2) and *curvedness* (3) in the range of –0.356 (red) to 1.191 Å au (blue), –1.0 (concave) to 1.0 Å au (convex) and –4.0 (flat) to 0.4 Å au (singular), respectively (Figure 3A). In d_{norm} surface, strong hydrogen bonds result in bright-red spots near the hydrogen bonding acceptor and donor atoms, while other interactions result in faint-red spots. The d_{norm} mapped surfaces of the present investigated compound exhibit two interactions; the first interaction between

the oxygen atom of the sulfonyl group (S=O) and with the hydrogen atom of pyrimidine ring, which can be visualized as bright red spot and labeled as (i). The second interaction between the oxygen atom of sulfonyl group (S=O) and with the hydrogen atom of a methyl group (CH_3), which can be visualized as bright red spots and labeled as (ii) (Figure 3A and 3B).

From the decomposition of fingerprint plots of the title compound represents the major contributors contacts on the surface of Hirshfeld namely O···H/H···O and H···H contacts. The intermolecular hydrogen bonds contacts O···H /H··O have the greatest contribution to the surface of Hirshfeld (21.9%), they are represented by two sharp symmetric spikes in the two-dimensional fingerprint maps (Figure 3.C (a)). The H···H contacts appear in the middle of the scattered points in the two dimensional fingerprint maps; they comprise 6% of the entire surface of Hirshfeld (Figure 3.C (b)).

3.3. Optimization of geometry

The geometry optimization of DCMSP was carried out for an isolated molecule in the gas phase utilizing DFT calculations with the B3LYP correlation functional and 6-311++G (d,p) basis set using the Gaussian 09W software and those results are included in the supplementary data (supplementary data).

3.4. Vibrational Analysis

The calculated (scaled) wavenumbers, observed IR, Raman bands and assignments are given in Table 3. The methyl group stretching modes (asymmetric and symmetric) are expected in the region 3100-2900 cm^{-1} [69, 70]. Wherein these modes are observed at 3058 cm^{-1} in the IR spectrum, 3060 cm^{-1} in the Raman spectrum and 3064, 3043 cm^{-1} theoretically (asymmetric stretching modes); at 2946 cm^{-1} in the Raman spectrum and 2949 cm^{-1} theoretically (symmetric stretching modes) as expected [71]. In this work, the methyl group deformations bands have been observed at 1400 cm^{-1} in the IR spectrum, 1399 cm^{-1} in the Raman spectrum and 1395, 1392 cm^{-1} (DFT) (asymmetric deformation), 1297 cm^{-1} in the IR spectrum, 1298 cm^{-1} in Raman spectrum and 1301 cm^{-1} (DFT) (symmetric deformation) as expected [69].

Pyrimidine ring C-H stretching mode are calculated at 3114 cm^{-1} (DFT), while it has been observed experimentally at 3101 cm^{-1} in both IR and Raman spectrum and expected in the range 3000-3100 cm^{-1} [71]. This mode (mode number 1) is pure and PED is exactly 100% with IR intensity of 4.60 and Raman activity of 77.79. The in-plane and out-plane C-H deformation modes of the heteroaromatic ring are expected in the region 1300-1000 cm^{-1} and 1000-600 cm^{-1} respectively [71]. These bands are assigned at 1082 cm^{-1} (IR spectrum), 1357, 1083 cm^{-1} (Raman spectrum), 1356, 1084 cm^{-1} (DFT) (in-plane deformation) and 612 cm^{-1} (IR spectrum), 611 cm^{-1} (Raman spectrum), 605 cm^{-1} (DFT) (out-of-plane deformation).

The C=N stretching modes are assigned at 1363, 1255, 1198, 1082 cm^{-1} in the IR spectrum, 1357, 1258, 1214, 1083 cm^{-1} in the Raman spectrum and in the range 1356-1084 cm^{-1} theoretically, which are in agreement with reported values [72]. The modes observed at 1509, 1499 cm^{-1} theoretically, at 1512 cm^{-1} in the IR spectrum and at 1511 cm^{-1} in the Raman spectrum are assigned as the pyrimidine ring C=C stretching modes, which are in agreement with the literature values [73].

The C-Cl stretching vibrational modes are assigned at 800 cm^{-1} in the IR spectrum, 802 cm^{-1} in the Raman spectrum and computationally at 804, 789 cm^{-1}, with high IR intensity and low Raman activity, which are expected in the region 750-880 cm^{-1} [69] and in agreement with reported values at 800 cm^{-1} (IR) and 843, 818 (DFT) cm^{-1} [71].

The stretching vibrational modes of the SO_2 group observed at 1250 cm^{-1} (IR spectrum), 1246 cm^{-1} (Raman spectrum) and at 1245 cm^{-1} (DFT) (anti symmetric) and 1066 cm^{-1} (Raman spectrum), 1063 cm^{-1}(DFT) (symmetric) in agreement with reported values [74].

3.5. Frontier orbital analysis, Global reactivity parameters and electronic spectral analysis

Reactivity is an inherent property of the molecular system which reflects on the feasibility of chemical modification. The stability and reactivity of the molecular system are addressed through global reactivity parameters such as chemical potential, global hardness and electrophilicity index. Frontier molecular orbitals of the DCMSP are visualized in Figure 4 and the energy gap between the highest occupied molecular orbital (HOMO) and the lowest unoccupied molecular orbital (LUMO) is calculated using the DFT/B3LYP/6-311++G(d,p) level of theory. HOMO (molecular orbital number 57 with energy of –8.49 eV) is confined over the methylsulfonyl group, partially on pyrimidine ring, whereas the LUMO (molecular orbital number 58 with energy of –2.67 eV) is confined over the pyrimidine ring partially on sulfonyl group. This supports that eventual charge transfer occurs within the present investigated compound from methylsulfonyl group to pyrimidine ring, while the energy gap between frontier orbitals is 5.82 eV. The global reactivity parameters for present investigated molecule are: ionization potential (I) is equal to $-E_{HOMO}$ = 8.49 eV, electron affinity (A) E_{LUMO} = 2.67 eV, electronegativity $\chi = (I+A)/2$ = 5.58 eV, global hardness $\eta = (I-A)/2$ = 2.91 eV, chemical potential (μ) equals to $-(I+A)/2$ = –5.58 eV, chemical softness (ν) equals to $1/\eta$ = 0.34 eV and electrophilicity index (ω) = $\mu^2/2\eta$ = 5.34 eV [75, 76]. The maximum absorption wavelengths λ [nm], excitation energies E [eV] and oscillator strengths (f) of the title compound are computed using TD-DFT/B3LYP/6-311++G(d,p) method [33] (Table 4). The simulated UV-Visible spectrum in the gas phase is shown in Figure S3. The electronic

absorption spectra of title compound show an electronic absorption band with maxima at λ_{max} = 254 nm, which is good in agreement with theoretical value (λ_{max} at 253 nm).

3.6. NBO analysis

Natural bonding orbital analysis (NBO analysis) calculations were done with the help of NBO 3.1 program [77], as is implemented in a Gaussian 09W suite, at the DFT/B3LYP/6-311++G(d,p) level of theory. Second-order interactions obtained by NBO analysis are listed in Table 5 and Table 6. The important intermolecular hyper conjugative interactions are: C12-S9 from O11 of n2(O11)→ σ*(C12-S9),C12-S9 from O10 of n2(O10)→ σ*(C12-S9), N6-C1 from N2 of n1(N2) → σ*(N6-C1), N2-C1 from N6 of n1(N6) → σ*(N2-C1), with electrons densities 0.17263, 0.17263, 0.03712, 0.04159e and stabilization energies 17.58, 17.58, 12.49, 13.01 kJ/mol. Almost 100% p-character was observed as lone pairs of n2O11 (99.85) and n2O10 (99.85).

3.7. Nonlinear optical properties

The SM approach was used in the calculations of the electrical properties of the embedded molecule DCMSP, as is indicated in Table 7. The μ_y component of the dipole moment was the one with the highest contribution to the total dipole moment, whereas the μ_x component contributed the least. The value of the total dipole moment (μ) due to the effect of the ambient polarization was 5.71 D. The calculated linear polarizability in the case static for the crystalline phase DCMSP was 17.34×10^{-24} esu and the component that contributed mostly to the value of the average polarizability was α_{zz}, while the one that contributed the least was α_{yz}. The values of the second hyperpolarizability can be seen in Table 7 for the embedded molecule DCMSP. The tensor components γ_{xxxx} and γ_{zzzz} showed a greater participation in the calculation of the average of the second hyperpolarizability $\bar{\gamma}$.

From Eq. (4) the static linear refractive index estimated for DCMSP crystal is n_o = 1.58 and the Eq. (5) was used to calculate the third order $\chi^{(3)}$ electric susceptibility of the DCMSP crystal and value found for $\chi^{(3)}$ in the static case for the DCMSP crystal was 34.02×10^{-22} $(m/V)^2$. However, in order to make a proper comparison between the DFT predictions and the experimental value of $\chi^{(3)}$ measured by the single Z-scan technique [14], we have find a first estimate of the frequency-dependent second hyperpolarizability ($\langle\gamma(-\omega;\omega,\omega,-\omega)\rangle$) associated with a nonlinear optical process [78] of the intensity-dependent refractive index (IDRI) of the dc-K results. According to previous work [79], for small frequencies [80], ($\langle\gamma(-\omega;\omega,\omega,-\omega)\rangle$ can be written as $\langle\gamma(-\omega;\omega,\omega,-\omega)\rangle \cong 2\langle\gamma(-\omega;\omega,0,0)\rangle - \langle\gamma(0;0,0,0)\rangle$ details in Table 8. The linear refractive index dispersion curves and the third-

order nonlinear optical susceptibility $\chi^{(3)}$ for the DCMSP crystal are shown in Figure 5. In both figures the linear refractive index and the $\chi^{(3)}$ show similar behavior as a function of frequency. Table 9 presents the DFT prediction and the experimental results of the macroscopic quantities studied. The value of DCMSP crystal is therefore 24.67, 28.51, and 23.94 times higher respectively than the values found experimentally by D'silva et al. [14], see Table 9.

3.8. MEP and ALIE surfaces, atomic Fukui indices

The identification of reactive molecular sites of DCMSP molecule in this work has been done firstly by a combination of MEP and ALIE quantum molecular descriptors. Both of these descriptors are widely used for the determination of molecular areas which are sensitive towards electrophilic and nucleophilic attacks [81-86]. Although MEP descriptor is used somewhat more frequently, ALIE descriptor might better perform when it comes to the identification of sites prone to electrophilic attacks [87-90]. Both MEP and ALIE descriptors are most frequently visualized by a mapping of their values to the electron density surface, which is the method adopted in this work as well. DCMSP molecule's MEP and ALIE surfaces have been provided in Figure 6.

According to the provided MEP surface of DCMSP molecule, the oxygen atoms are recognized as sensitive towards electrophilic attacks, due to the fact that MEP has the lowest values precisely at these locations. Maximal MEP values are located in near vicinities of hydrogen atoms and above chlorine atoms, designating these locations as possibly sensitive towards nucleophilic attacks. On the other side, ALIE descriptor identifies the near vicinity of nitrogen atom N6 as possibly sensitive towards the electrophilic attacks. Similarly, as in the case of the MEP descriptor, maximal ALIE values are located in near vicinities of hydrogen atoms and above chlorine atoms.

The concept of Fukui functions is very frequently employed for the further assessment of local reactive properties of molecular structures. Besides Fukui functions, Fukui indices are also frequently used. Sometimes, this descriptor is called condensed-to-atom Fukui function. In Jaguar program for DFT calculations, Fukui indices are calculated according to methodologies explained in references [91, 92]. In this particular work we have used $f_{\mathrm{NN}}^{\mathrm{HOMO}}$ and $f_{\mathrm{NN}}^{\mathrm{LUMO}}$ indices for further understanding of local reactive properties of DCMSP molecule. Fukui indices have been summarized for DCMSP molecule in Figure 7.

In Figure 7, the very low (and therefore irrelevant) values of Fukui indices haven't been visualized for the sake of clarity. The high values of $f_{\mathrm{NN}}^{\mathrm{HOMO}}$ index indicate that certain atom

might donate electrons, thanks to which it can be stated that it is prone to electrophilic attacks. According to Figure 7a, the highest positive values of the $f_{\mathrm{NN}}^{\mathrm{HOMO}}$ index have been calculated for oxygen atoms. These results are in agreement with the conclusions of MEP surfaces. On the other side, the high values of $f_{\mathrm{NN}}^{\mathrm{LUMO}}$ index indicate that atom might receive electrons and therefore might be sensitive towards the nucleophilic attacks. According to Figure 7b, the highest values of the $f_{\mathrm{NN}}^{\mathrm{LUMO}}$ index have been calculated for carbon atoms C1 and C4, designating them as possibly vulnerable to nucleophilic attacks.

3.9. Sensitivity towards autoxidation and water

Taking into account that autoxidation mechanism belongs to a group of very important reactions from the industrial aspects [18, 83, 85, 93-95], we have calculated BDE and H-BDE values for all single acyclic bonds of DCMSP molecule. Concretely, H-BDE values reflect the sensitivity of molecule towards the autoxidation mechanism and this fact is very important because experimental measurements of BDE are very difficult and time-consuming [20, 96]. For instance, if the H-BDE value is calculated to be in the range between 70 and 85 kcal/mol, then there is a high possibility that the observed molecule is sensitive towards the autoxidation mechanism [96]. H-BDE values from 85 kcal/mol up to 90 kcal/mol might also be important, but they have to be taken into account with caution [97]. BDE values for the remaining single acyclic bonds don't have particular importance for a prediction of sensitivity towards autoxidation mechanism, but they might serve for the comparison of bond strengths within the molecule. BDEs and H-BDEs for DCMSP molecule have been summarized in Figure 8.

According to the H-BDE values calculated for DCMSP molecule, it can be stated that this molecule is highly stable towards the autoxidation mechanism due to the fact that all of the H-BDE values are much higher than the upper border level of 90 kcal/mol. This indicates a high stability of DCMSP in the presence of oxygen, difficult degradation and therefore long shelf life of formulations based on it. On the other side, the lowest BDE value has been calculated for the single bond connecting the sulphur atom and the five-membered ring, indicating that degradation of DCMSP molecule might start by breaking this bond.

MD simulation has been performed and radial distribution functions (RDF) have been calculated for all atoms in order to identify the atoms with the pronounced interactions with water molecules. RDFs have been calculated with respect to the distance between the observed atom and oxygen atom of water molecules. Representative RDFs with respect to their profile have been presented in Figure 9.

According to results related to RDFs, DCMSP molecule has significant stability in water since there are no hydrogen atoms with their maximal g(r) values located at distances below 2 Å. The highest g(r) values have been calculated for both chlorine atoms, with distances of about 3.5 Å. High maximal g(r) values have also been calculated for sulphur atom and carbon atom C12, however, their maximal g(r) values are also located at high distances, especially in the case of case of the sulphur atom with a distance of 4 Å. These results indicate a very low possibility for DCMSP's degradation to be triggered by natural environmental conditions.

3.10. NMR spectroscopy analysis

Nuclear magnetic resonance spectroscopy (NMR spectroscopy) is one of the powerful spectroscopic techniques for the identification of structure as well as functional groups of chemical species. For title compound, ^{1}H and ^{13}C-NMR chemical shift values were recorded in a DMSO-d_6 solvent and TMS as internal standard on Bruker FT-NMR spectrometer operating at 400 MHz (Figure S4) and theoretically calculated by GIAO method [32] using DFT/6-311++G(d,p) basic set, which is performed after full geometry optimization. The chemical shift values of the proton spectra were observed in two regions; the first signal observed at 8.4/7.7 ppm (experimental/DFT) for aromatic proton and another signal observed for methyl proton at 3.4/3.1 ppm (experimental/DFT). Chemical shift values of ^{13}C-NMR of typical organic molecule usually >100 ppm [98, 99], for title compound aromatic carbons were observed in the range (experimental/DFT) 125-164/130-177 ppm. The chemical shift value for both C3 and C5 is 162/177 (experimental/DFT) were found to be significantly high due to the impact of the electronegative chlorine atom. For the methyl group, carbon (C12) signal is observed at the upfield region (experimental/DFT) at 40/45 ppm (Table S1).

3.11. Mulliken atomic charge analysis

The calculation and analysis of Mulliken atomic charges have an important role for the determination of reactive properties of the studied molecular systems. Atomic charge affects the dipole moment, polarizability, electronic structure and other molecular properties of the system [100]. The Mulliken atomic charges of DCMSP are obtained by means of Mulliken population analysis and those results are tabulated in Table S2. The charges at the sites of the C atoms attached to the electronegative atoms N, S and Cl atoms are positive because of the electron-withdrawing nature of N, S and Cl atoms. Thus, C_1, C_3 and C_5 atoms accommodate positive charge and become more acidic. Other C atoms are in negative charge. Moreover, Mulliken atomic charges also indicate that all of the hydrogen atoms have a net positive charge, but the H_{13} and H_{14} atoms accommodate more positive atomic charges 0.162 and 0.183 e, than the other hydrogen atoms and therefore are considered as acidic. The calculated

Mulliken charges of O_{10} and O_{11}, H_{13}, H_{14}, C_4 and C_{12} atoms are –0.480, –0.480, 0.162, 0.183, –0.002 and –0.432 e, respectively, and these values confirm the existence of C-H···O intermolecular hydrogen bond in solid forms.

4. Conclusions

The title compound DCMSP was synthetized and characterized by SCXRD, FT-IR, FT-Raman, ^{1}H and ^{13}C-NMR spectroscopic signature studies. DFT calculation and MD simulation studies were used for to predict reactive properties and stability of title compound. The experimental geometrical parameters were good in agreement with predicted geometrical parameters. The DCMSP crystal macroscopic quantities such as the linear refractive index (n = 1.613) and the third-order nonlinear susceptibility ($\chi^{(3)}(-\omega;\omega,\omega,-\omega) = 56.74\times10^{-22}\ \mathrm{m^2/V^2}$) were calculated from the Clausius-Mossoti equation. This $\chi^{(3)}$ value is twenty eight times greater than the reported values for others chalcone derivatives (see Table 9), qualifying the DCMSP crystal as a potential candidate for application in nonlinear optical devices. The SM approach was successfully used to estimate the third-order nonlinear susceptibility and the linear refractive index in Ref. [101] with results close to the experimental ones. MEP surfaces showed that oxygen atoms might be sensitive towards electrophilic attacks. On the other side, ALIE surfaces also indicated nitrogen atom N6 to be possibly sensitive towards electrophilic attacks. The results of $f_{\mathrm{NN}}^{\mathrm{HOMO}}$ atomic Fukui index are in agreement with the findings of MEP surfaces regarding the sensitivity of oxygen atoms towards electrophilic attacks, while $f_{\mathrm{NN}}^{\mathrm{LUMO}}$ atomic Fukui index highlighted two carbon atoms of five membered ring to be possible prone to nucleophilic attacks. H-BDE values indicated stability towards the autoxidation mechanism, while BDE values indicated that degradation of DCMSP might start by breaking of C1–S9 bond. MD simulation and RDFs showed that DCMSP is stable in water as well, with all representative atoms having maximal g(r) values at distances beyond 3 Å.

Acknowledgment

The author C. Valverde thank the Brazilian funding agencies CAPES, CNPq, and FAPEG for financial support and the PrP/UEG for the research developed with the support of the UEG High Performance Computing Nucleus. Part of this study was conducted within the projects supported by the Ministry of Education, Science and Technological Development of Serbia, grant numbers III41017. Part of this work has been performed thanks to the support received from Schrödinger Inc.

Supplementary Material

The cif file of the title compound have been assigned CCDC number 1863699 and can be obtained free of cost on application to CCDC 12 Union Road, Cambridge CB21 EZ, UK. (Fax: (+44) 1223 336-033: e-mail: data_request@ccdc.cam.ac.uk).

References

[1] G. Shi, Y. Wang, F. Zhang, B. Zhang, Z. Yang, X. Hou, S. Pan, K.R. Poeppelmeier, Finding the Next Deep-Ultraviolet Nonlinear Optical Material: $NH_4B_4O_6F$, J. Am. Chem. Soc. 139 (2017) 10645–10648.

[2] B. Zhang, G. Shi, Z. Yang, F. Zhang, S. Pan, Fluorooxoborates: Beryllium-Free Deep-Ultraviolet Nonlinear Optical Materials without Layered Growth, Angew. Chemie Int. Ed. 56 (2017) 3916–3919.

[3] M. Mutailipu, M. Zhang, B. Zhang, L. Wang, Z. Yang, X. Zhou, S. Pan, $SrB_5O_7F_3$ Functionalized with $[B_5O_9F_3]^{6-}$ Chromophores: Accelerating the Rational Design of Deep-Ultraviolet Nonlinear Optical Materials, Angew. Chemie Int. Ed. 57 (2018) 6095–6099.

[4] E. Timurdogan, C. V Poulton, M.J. Byrd, M.R. Watts, Electric field-induced second-order nonlinear optical effects in silicon waveguides, Nat. Photonics. 11 (2017) 200-2006.

[5] L. Lu, Z. Liang, L. Wu, Y. Chen, Y. Song, S.C. Dhanabalan, J.S. Ponraj, B. Dong, Y. Xiang, Few-layer Bismuthene: Sonochemical Exfoliation, Nonlinear Optics and Applications for Ultrafast Photonics with Enhanced Stability, Laser & Photonics Reviews, 12 (2018) 1700221.

[6] R. Salvi, C. Cerqueira-coutinho, E. Ricci-junior, N. Santos, S.R. Pinto, E.S. Bernardes, P. Lopes, B. De Araujo, R. Santos-oliveira, Diagnosing lung cancer using etoposide microparticles labeled with ^{99m}Tc, Artif Cells Nanomed Biotechnol. 46(2) (2018) 341-345.

[7] M. Luo, F. Liang, Y. Song, D. Zhao, F. Xu, N. Ye, Z. Lin, M. Luo, F. Liang, Y. Song, D. Zhao, F. Xu, N. Ye, Z. Lin, $M_2B_{10}O_{14}F_6$ (M = Ca, Sr): Two Noncentrosymmetric Alkaline Earth Fluorooxoborates as Promising Next-Generation Deep-Ultraviolet Nonlinear Optical Materials, J Am Chem Soc. 140 (11) (2018) 3884-3887.

[8] H. Zhao, S. Han, R. Hui, Nonlinear Optical Spectroscopy of Two-Dimensional Materials Qiannan Cui, (2017).

[9] M. Nakano, Open-Shell-Character-Based Molecular Design Principles : Applications to Nonlinear Optics and Singlet Fission, Chem Rec. 17 (2017) 27-62.

[10] R. Mallah, M.C. Sreenath, S. Chitrambalam, I.H. Joe, N. Sekar, Excitation energy transfer processes in BODIPY based donor-acceptor system - Synthesis, photophysics, NLO and DFT study, Opt. Mater. 84 (2018) 795–806.

[11] M. Anis, G.G. Muley, V.G. Pahurkar, M.I. Baig, S.R. Dagdale, Influence of Nd^{+3} on zinc tris-thioureasulphate single crystal : A comparative crystal growth, structural , linear – nonlinear optical and dielectric study to explore NLO device applications, Materials Research Innovations, DOI: 10.1080/14328917.2016.1264848.

[12] Joel M. Hales, Shijun Zheng, Stephen Barlow, A. Seth R. Marder, J.W. Perry, Bisdioxaborine Polymethines with Large Third-Order Nonlinearities for All-Optical Signal Processing, (2006). doi:10.1021/JA063535M.

[13] S.R. Marder, B. Kippelen, A.K.-Y. Jen, N. Peyghambarian, Design and synthesis of chromophores and polymers for electro-optic and photorefractive applications, Nature. 388 (1997) 845–851. doi:10.1038/42190.

[14] E.D. D'silva, G.K. Podagatlapalli, S. VenugopalRao, S.M. Dharmaprakash, Study on third-order nonlinear optical properties of 4-methylsulfanyl chalcone derivatives using picosecond pulses, Mater. Res. Bull. 47 (2012) 3552–3557.

[15] S. Shettigar, G. Umesh, K. Chandrasekharan, B.K. Sarojini, B. Narayana, Studies on third-order nonlinear optical properties of chalcone derivatives in polymer host, Opt. Mater. 30 (2008) 1297–1303.

[16] A. John Kiran, A. Mithun, B. ShivaramaHolla, H.D. Shashikala, G. Umesh, K. Chandrasekharan, Nonlinear optical studies of 1-3-diaryl-propenones containing 4-methylthiophenyl moieties, Opt. Commun. 269 (2007) 235–240.

[17] A.N. Prabhu, V. Upadhyaya, A. Jayarama, K.S. Bhat, Third-order NLO property of thienylchalcone derivative: Physicochemical analysis and crystal structure determination, Mol. Cryst. Liq. Cryst. 637 (2016) 76–86.

[18] S. Armaković, S.J. Armaković, B.F. Abramović, Theoretical investigation of loratadine reactivity in order to understand its degradation properties: DFT and MD study, Journal of molecular modelling, 22(10) (2016) 240.

[19] E.I. Izgorodina, Z.L. Seeger, D.L. Scarborough, S.Y. Tan, Quantum Chemical Methods for the Prediction of Energetic, Physical, and Spectroscopic Properties of Ionic Liquids. (2017).

[20] P. Lienard, J. Gavartin, G. Boccardi, M. Meunier, Predicting drug substances autoxidation, Pharmaceutical research, 32(1) (2015) 300-310.

[21] A. Reisi-Vanani, M. Safipoor, Investigation of carbon monoxide adsorption onto sumanene (C21H12) decorated with Li^+ ions toward its elimination, Current Applied Physics, 17(11) (2017)1382-1395.

[22] A. Reisi-Vanani, Z. Shabani, Evaluation of the hydrogen adsorption onto Li and Li^+ decorated circumtrindene (C36H12): A theoretical study, International Journal of Hydrogen Energy, 42(36) (2017) 22973-22986.

[23] S. Armaković, S.J. Armaković, S. Koziel, Optoelectronic properties of curved carbon systems, Carbon, 111 (2017) 371-379.

[24] G.M. Sheldrick, A short history of SHELX, Acta Cryst. A64 (2008) 112-122.

[25] A.L. Spek, Structure validation in chemical crystallography, ActaCrystallogr., D 65 (2009) 148-155.

[26] L.J. Farrugia, WinGX suite for small-molecule single-crystal crystallography, J. Appl. Crsystallogr. 32 (1999) 837-838.

[27] C.F. Macrae, I.J. Bruno, J.A. Chisholm, P.R. Edgington, P. McCabe, E. Pidcock, L. Rodriguez-Monge, R. Taylor, J. van de Streek, P.A. Wood, Mercury CSD 2.0 - New Features for the Visualization and Investigation of Crystal Structures, J. Appl. Cryst., 41 (2008) 466-470.

[28] Gaussian 09, Revision B.01, M.J. Frisch, G.W. Trucks, H.B. Schlegel, G.E. Scuseria, M.A. Robb, J.R. Cheeseman, G. Scalmani, V. Barone, B. Mennucci, G.A. Petersson, H. Nakatsuji, M. Caricato, X. Li, H.P. Hratchian, A.F. Izmaylov, J. Bloino, G. Zheng, J.L. Sonnenberg, M. Hada, M. Ehara, K. Toyota, R. Fukuda, J. Hasegawa, M. Ishida, T. Nakajima, Y. Honda, O. Kitao, H. Nakai, T. Vreven, J.A. Montgomery, Jr., J.E. Peralta, F. Ogliaro, M. Bearpark, J.J. Heyd, E. Brothers, K.N. Kudin, V.N. Staroverov, T. Keith, R. Kobayashi, J. Normand, K. Raghavachari, A. Rendell, J.C. Burant, S.S. Iyengar, J. Tomasi, M. Cossi, N. Rega, J.M. Millam, M. Klene, J.E. Knox, J.B. Cross, V. Bakken, C. Adamo, J. Jaramillo, R. Gomperts, R.E. Stratmann, O. Yazyev, A.J. Austin, R. Cammi, C. Pomelli, J.W. Ochterski, R.L. Martin, K. Morokuma, V.G. Zakrzewski, G.A. Voth, P. Salvador, J.J. Dannenberg, S. Dapprich, A.D. Daniels, O. Farkas, J.B. Foresman, J.V. Ortiz, J. Cioslowski, D.J. Fox, Gaussian, Inc., Wallingford CT, 2010.

[29] Materials Science Suite 2018-1, Schrödinger, LLC, New York, NY. 2018.

[30] A.D. Becke, Density-functional thermochemistry. III. The role of exact exchange, The Journal of Chemical Physics, 98(7) (1993) 5648-5652.

[31] Michal. H. Jamroz, Vibrational Energy Distribution Analysis VEDA4, Warsaw, 2004-2010.

[32] J.B. Foresman, Pittsburg, PA, in: E. Frisch (Ed.), Exploring Chemistry with Electronic Structure Methods: a Guide to Using Gaussian, 1996.

[33] R. Ditchfield, Molecular orbital theory of magnetic shielding and magnetic susceptibility, J. Chem. Phys. 56 (1972) 5688–5691.

[34] F. Furche, R. Ahlrichs, Adiabatic time dependent density functional methods for excited states properties, J. Chem. Phys. 117 (2002) 7433-7447.

[35] M.A. Spackman, P. Munshi, D. Jayatilaka, The use of dipole lattice sums to estimate electric fields and dipole moment enhancement in molecular crystals, Chem. Phys. Lett. 443 (2007) 87–91.

[36] O.L. Santos, J.R. Sabino, H.C. Georg, T.L. Fonseca, M.A. Castro, Electric properties of the 3-methyl-4-nitropyridine-1-oxyde (POM) molecules in solid phase: A theoretical study including environment polarization effect, Chem. Phys. Lett. 669 (2017) 176–180.

[37] T.L. Fonseca, J.R. Sabino, M.A. Castro, H.C. Georg, A theoretical investigation of electric properties of <scp>L</scp> -arginine phosphate monohydrate including environment polarization effects, J. Chem. Phys. 133 (2010) 144103.

[38] O.L. Santos, T.L. Fonseca, J.R. Sabino, H.C. Georg, M.A. Castro, Polarization effects on the electric properties of urea and thiourea molecules in solid phase, J. Chem. Phys. 143 (2015) 234503.

[39] J.M.F. Custodio, F.G. Santos, W.F. Vaz, C.E.P. Cunha, R.G. Silveira, M.M. Anjos, C.E.M. Campos, G.R. Oliveira, F.T. Martins, C.C. da Silva, C. Valverde, B. Baseia, H.B. Napolitano, Molecular structure of hybrid imino-chalcone in the solid state: X-ray diffraction, spectroscopy study and third-order nonlinear optical properties, J. Mol. Struct. 1157 (2018).

[40] C. Valverde, W.F. Vaz, J.M.F. Custodio, V.S. Duarte, P.S. Carvalho-Jr, A.S. Figueredo, G.L.B. de Aquino, B. Baseia, H.B. Napolitano, The solid state structure and environmental polarization effect of a novel asymmetric azine, New J. Chem. 41 (2017) 11361–11371.

[41] B. Baseia, F. Osório, L. Lima, C. Valverde, Effects of Changing Substituents on the Non-Linear Optical Properties of Two Coumarin Derivatives, Crystals. 7 (2017) 158.

[42] A.N. Castro, F.A.P. Osório, R.R. Ternavisk, H.B. Napolitano, C. Valverde, B. Baseia, Theoretical investigations of nonlinear optical properties of two crystalline acetamides

structures including polarization effects of their environment, Chem. Phys. Lett. 681 (2017) 110–123.

[43] R.F.N. Rodrigues, L.R. Almeida, F.G. dos Santos, P.S. Carvalho Jr, W.C. de Souza, K.S. Moreira, G.L.B. de Aquino, C. Valverde, H.B. Napolitano, B. Baseia, Solid state characterization and theoretical study of non-linear optical properties of a Fluoro-N-Acylhydrazide derivative, PLoS One. 12 (2017) e0175859.

[44] W.F. Vaz, J.M.F. Custodio, R.G. Silveira, A.N. Castro, C.E.M. Campos, M.M. Anjos, G.R. Oliveira, C. Valverde, B. Baseia, H.B. Napolitano, Synthesis, characterization, and third-order nonlinear optical properties of a new neolignane analogue, RSC Adv. 6 (2016) 79215–79227.

[45] L.R. Almeida, M.M. Anjos, G.C. Ribeiro, C. Valverde, D.F.S. Machado, G.R. Oliveira, H.B. Napolitano, H.C.B. de Oliveira, Synthesis, structural characterization and computational study of a novel amino chalcone: a potential nonlinear optical material, New J. Chem. 41 (2017) 1744–1754.

[46] J. Custodio, C. Moreira, C. Valverde, G. de Aquino, B. Baseia, H. Napolitano, Hirshfeld Surfaces and Nonlinear Optics on Two Conformers of a Heterocyclic Chalcone, J. Braz. Chem. Soc. (2017) 168–179.

[47] C. Valverde, R.F.N. Rodrigues, D.F.S. Machado, B. Baseia, H.C.B. de Oliveira, Effect of the crystalline environment on the third-order nonlinear optical properties of L-arginine phosphate monohydrate: a theoretical study, J. Mol. Model. 23 (2017) 122.

[48] G.C. Ribeiro, L.R. Almeida, H.B. Napolitano, C. Valverde, B. Baseia, Polarization effects on the third-order nonlinear optical properties of two polymorphs of enamine derivative, Theor. Chem. Acc. 135 (2016) 244.

[49] A.N. Castro, L.R. Almeida, M.M. Anjos, G.R. Oliveira, H.B. Napolitano, C. Valverde, B. Baseia, Theoretical study on the third-order nonlinear optical properties and structural characterization of 3-Acetyl-6-Bromocoumarin, Chem. Phys. Lett. 653 (2016) 122–130.

[50] D.A. Kleinman, Nonlinear Dielectric Polarization in Optical Media, Phys. Rev. 126 (1962) 1977–1979.

[51] A.D.Bochevarov, E. Harder, T.F. Hughes, J.R. Greenwood, D.A. Braden, D.M. Philipp, D. Rinaldo, M.D. Halls, J. Zhang, R.A. Friesner, Jaguar: A high-performance quantum chemistry software program with strengths in life and materials sciences, International Journal of Quantum Chemistry, 113(18) (2013) 2110-2142.

[52] Schrödinger Release 2017-4: Jaguar, Schrödinger, LLC, New York, NY, 2017. 2017.

[53] L.D. Jacobson, A.D. Bochevarov, M.A. Watson, T.F. Hughes, D. Rinaldo, S. Ehrlich, T.B. Steinbrecher, S. Vaitheeswaran, D.M. Philipp, M.D. Halls, Automated Transition State Search and Its Application to Diverse Types of Organic Reactions, Journal of chemical theory and computation, 13(11) (2017) 5780-5797.

[54] D. Shivakumar, J. Williams, Y. Wu, W. Damm, J. Shelley, W. Sherman, Prediction of absolute solvation free energies using molecular dynamics free energy perturbation and the OPLS force field, Journal of chemical theory and computation, 6(5) (2010) 1509-1519.

[55] Z. Guo,U. Mohanty, J. Noehre, T.K. Sawyer, W. Sherman, G. Krilov, Probing the α-helical structural stability of stapled p53 peptides: molecular dynamics simulations and analysis, Chemical biology & drug design, 75(4) (2010) 348-359.

[56] K.J.Bowers, E. Chow, H. Xu, R.O. Dror, M.P. Eastwood, B.A. Gregersen, J.L. Klepeis, I. Kolossvary, M.A. Moraes, F.D. Sacerdoti, Scalable algorithms for molecular dynamics simulations on commodity clusters, in Proceedings of the 2006 ACM/IEEE conference on Supercomputing, 2006, ACM.

[57] Materials Science Suite 2017-2, Schrödinger, LLC, New York, NY, 2017.

[58] E.Harder, W. Damm, J. Maple, C. Wu, M. Reboul, J.Y. Xiang, L. Wang, D. Lupyan, M.K. Dahlgren, J.L. Knight, OPLS3: a force field providing broad coverage of drug-like small molecules and proteins, Journal of Chemical Theory and Computation, 12(1) (2015) 281-296.

[59] W.L.Jorgensen,D.S. Maxwell, J. Tirado-Rives, Development and testing of the OPLS all-atom force field on conformational energetics and properties of organic liquids, Journal of the American Chemical Society, 118(45) (1996) 11225-11236.

[60] W.L. Jorgensen, J. Tirado-Rives, The OPLS [optimized potentials for liquid simulations] potential functions for proteins, energy minimizations for crystals of cyclic peptides and crambin, Journal of the American Chemical Society, 110(6) (1988) 1657-1666.

[61] H.J. Berendsen, J.P. Postma, W.F. van Gunsteren, J. Hermans, Interaction models for water in relation to protein hydration, in Intermolecular forces, Springer,1981, pp. 331-342.

[62] M.A. Spackman, D. Jayatilaka, Hirshfeld surface analysis, CrystEngComm. 11 (2009) 19-32.

[63] F.L. Hirshfeld, Bonded-Atom Fragments for Describing Molecular Charge Densities, Theor. Chim.Acta 44 (1977) 129-138.

[64] H.F. Clausen, M.S. Chevallier, M.A. Spackman, B.B. Iversen, Three new co-crystals of hydroquinone: crystal structures and Hirshfeld surface analysis of intermolecular interactions, New J. Chem. 34 (2010) 193-199.

[65] A.L. Rohl, M. Moret, W. Kaminsky, K. Claborn, J.J. McKinnon, B. Kahr, Hirshfeld surfaces identify inadequacies in computations of intermolecular interactions in crystals: pentamorphic 1, 8-dihydroxyanthraquinone, Cryst. Growth Des. 8 (2008) 4517-4525.

[66] A. Parkin, G. Barr, W. Dong, C.J. Gilmore, D. Jayatilaka, J.J. McKinnon, M.A. Spackman, C.C. Wilson, Comparing entire crystal structures: structural genetic fingerprinting, CrystEngComm. 9 (2007) 648-652.

[67] M.A. Spackman, J.J. McKinnon, Fingerprinting intermolecular interactions in molecular crystals, CrystEngComm. 4 (2002) 378-392.

[68] S.K. Wolff, D.J. Grimwood, J.J. McKinnon, D. Jayatilaka, M.A. Spackman, Crystal Explorer 2.0; University of Western Australia, Australia, 2012.

[69] N.P.G. Roeges, A Guide to the Complete Interpretation of Infrared Spectra of Organic Structures, John Wiley and Sons Inc., New York, 1994.

[70] R.M. Silverestein, G.C. Bassler, T.C. Morril, Spectroscopic Identification of Organic Compounds, fifth ed., John Wiley and Sons Inc., Singapore, 1991.

[71] V. Balachandran, A. Lakshmi, A. Janaki, vibrational spectroscopic studies and natural bond orbital analysis of 4,6-dichloro-2-(methylthio)-pyrimidine on density functional theory, SpectrochimicaActa Part A 81 (2011) 1-7.

[72] N.G. Haress, A.A. El-Emam, O.A. Al-Deeb, C.Y. Panicker, A.A. Al-Saadi, C. Van Alsenoy, J.A. War, S.K. Srivastava, Vibrational spectroscopic and molecular docking study of 2-Benzylsulfanyl-4-[(4-methylphenyl)-sulfanyl]-6-pentylpyrimidine-5-carbonitrile, a potential chemotherapeutic agent, SpectrochemActa A, 137 (2015) 569-80.

[73] S. Gunasekaran, S.R. Varadhan, K. Manoharan, Asian J.Phys. 12 (1993) 119-121.

[74] P. Krishna Murthy, V. Suneetha, Stevan Armaković, Sanja J. Armaković, P.A. Suchetan, L. Giri, R. Sreenivasa Rao, Synthesis, characterization and computational

study of the newly synthetized sulfonamide molecule, Journal of Molecular Structure, 1153 (2018) 212-229.

[75] T.A. Koopmans, Uber die zuordnung von wellenfunktionen und eigenwertenzu den einzelnenelektroneneines atoms, Physica 1 (1993) 104-113.

[76] R.J. Parr, L.V. Szentpaly, S. Liu, Electrophilicity index, J. Am. Chem. Soc. 121 (1999) 1922-1924.

[77] E.D. Glendening A.E. Reed, J.E. Carpenter, F. Weinhold, NBO Version 3.1, Gaussian Inc., Pittsburgh, PA, 2003.

[78] M. Maldonado, H.T.M.C.M. Baltar, A.S.L. Gomes, R. Vaia, K. Park, J. Che, M. Hsiao, C.B. de Araújo, A. Baev, P.N. Prasad, Coupled-plasmon induced optical nonlinearities in anisotropic arrays of gold nanorod clusters supported in a polymeric film, J. Appl. Phys. 121 (2017) 143103.

[79] S. Marques, M.A. Castro, S.A. Leão, T.L. Fonseca, Second hyperpolarizability of the calcium-doped lithium salt of pyridazine Li–$H_3C_4N_2$ ⋯ Ca, Chem. Phys. Lett. 659 (2016) 76–79.

[80] D.M. Bishop, D.W. De Kee, The frequency dependence of nonlinear optical processes, J. Chem. Phys. 104 (1996) 9876–9887.

[81] S. Armaković, S.J. Armaković, J.P. Šetrajčić, I.J. Šetrajčić, Active components of frequently used β-blockers from the aspect of computational study, Journal of molecular modeling, 18(9) (2012) 4491-4501.

[82] N. Okulik, A.H. Jubert, Theoretical study on the structure and reactive sites of three non-steroidal anti-inflammatory drugs: Ibuprofen, Naproxen and Tolmetin acids, Journal of Molecular Structure: THEOCHEM, 769(1) (2006) 135-141.

[83] P. Politzer, J.S. Murray, The fundamental nature and role of the electrostatic potential in atoms and molecules, Theoretical Chemistry Accounts, 108(3) (2002) 134-142.

[84] Y.S. Mary, V. Aswathy, C.Y. Panicker, A. Bielenica, P. Brzózka, O. Savczenko, S. Armaković, S.J. Armaković, C. Van Alsenoy, Spectroscopic, single crystal XRD structure, DFT and molecular dynamics investigation of 1-(3-chloro-4-fluorophenyl)-3-[3-(trifluoromethyl) phenyl] thiourea, RSC Advances, 6(113) (2016) 111997-112015.

[85] B. Sureshkumar, Y.S. Mary, C.Y. Panicker, S. Suma, S. Armaković, S.J. Armaković, C. Van Alsenoy, B. Narayana, Quinoline derivatives as possible lead compounds for

anti-malarial drugs: Spectroscopic, DFT and MD study, Arabian Journal of Chemistry, 2017.

[86] J.A. War, K. Jalaja, Y.S. Mary, C.Y. Panicker, S. Armaković, S.J. Armaković, S.K. Srivastava, C. Van Alsenoy, Spectroscopic characterization of 1-[3-(1H-imidazol-1-yl) propyl]-3-phenylthiourea and assessment of reactive and optoelectronic properties employing DFT calculations and molecular dynamics simulations, Journal of Molecular Structure, 1129 (2017) 72-85.

[87] J.S. Murray, J.M. Seminario, P. Politzer, P. Sjoberg, Average local ionization energies computed on the surfaces of some strained molecules, International Journal of Quantum Chemistry, 38(S24) (1990) 645-653.

[88] P. Politzer, F. Abu-Awwad, J.S. Murray, Comparison of density functional and Hartree–Fock average local ionization energies on molecular surfaces, International journal of quantum chemistry, 69(4) (1998) 607-613.

[89] F.A. Bulat, A. Toro-Labbé, T. Brinck, J.S. Murray, P. Politzer, Quantitative analysis of molecular surfaces: areas, volumes, electrostatic potentials and average local ionization energies, Journal of molecular modeling, 16(11) (2010) 1679-1691.

[90] P. Politzer, J.S. Murray, F.A. Bulat, Average local ionization energy: a review. Journal of molecular modeling, 16(11) (2010) 1731-1742.

[91] R.R. Contreras, P. Fuentealba, M. Galván, P. Pérez, A direct evaluation of regional Fukui functions in molecules, Chemical physics letters, 304(5) (1999) 405-413.

[92] E. Chamorro, P. Pérez, Condensed-to-atoms electronic Fukui functions within the framework of spin-polarized density-functional theory, The Journal of chemical physics, 123(11) (2005) 114107.

[93] S. Armaković, S. Armaković, N. Finčur, F. Šibul, D. Vione, J. Šetrajčić, B. Abramović, Influence of electron acceptors on the kinetics of metoprololphotocatalytic degradation in TiO2 suspension, A combined experimental and theoretical study, RSC Advances, 5(67) (2015) 54589-54604.

[94] S.J. Armaković, M. Grujić-Brojčin, M. Šćepanović, S. Armaković, A. Golubović, B. Babić, B.F. Abramović, Efficiency of La-doped TiO2 calcined at different temperatures in photocatalytic degradation of β-blockers, Arabian Journal of Chemistry, 2017.

[95] S.J. Armaković, S. Armaković, D.D. Četojević-Simin, F. Šibul, B.F. Abramović, Photocatalytic degradation of 4-amino-6-chlorobenzene-1, 3-disulfonamide stable

hydrolysis product of hydrochlorothiazide: Detection of intermediates and their toxicity, Environmental Pollution, 233 (2018) 916-924.

[96] T. Andersson, A. Broo, E. Evertsson, Prediction of Drug Candidates' Sensitivity Toward Autoxidation: Computational Estimation of C-H Dissociation Energies of Carbon-Centered Radicals, Journal of pharmaceutical sciences, 103(7) (2014) 1949-1955.

[97] G. Gryn'ova, J.L. Hodgson, M.L. Coote, Revising the mechanism of polymer autooxidation, Organic & biomolecular chemistry, 9(2) (2011) 480-490.

[98] H.O. Kalinowski, S. Brawn, Carbon13 NMR Spectroscopy, John Wiley and Sons, Chichester, 1988.

[99] K. Pinlajer, E. Kleinpeter (Eds.), Carbon13 Chemical Shifts in Structure and Spectrochemical Analysis, VCH publishers, Deerfield Beach, 1994.

[100] R.S. Mulliken, Electronic population analysis on LCAO-MO molecular wave functions, J. Chem. Phys. 23 (1955) 1833-1840.

[101] C. Valverde, F.A.P. Osório, T.L. Fonseca, B. Baseia, DFT study fo third-order nonlinear susceptibility of a chalcone crystal, Chem. Phys. Letters 706 (2018) 170–174.

Figures

Scheme -1: Synthetic scheme for 4,6-dichloro-2-(methylsulfonyl)pyrimidine.

Figure 1. Fourier transform Infra-Red spectrum of DCMSP.

Figure 2. Fourier transform Raman spectrum of DCMSP.

Figure 3. Analysis of 3D-Hirshfeld surfaces and 2D-finger print plots of DCMSP.

Figure 4. HOMO-LUMO plots of DCMSP.

Figure 5. Dynamic evolution of the studied values (a) of the linear refractive index and (b) third-order nonlinear optical susceptibility $\chi^{(3)}$ (in $10^{-22}\ \mathrm{m}^2/\mathrm{V}^2$) of the DCMSP crystal with respective values of frequencies.

Figure 6. MEP and ALIE surfaces of DCMSP.

Figure 7. Fukui indices for DCMSP molecule a) $f_{\mathrm{NN}}^{\mathrm{HOMO}}$ and b) $f_{\mathrm{NN}}^{\mathrm{LUMO}}$ indices.

Figure 8. H-BDE (red color) and BDE (blue color) values for DCMSP molecule.

Figure 9. Representative RDFs of DCMSP molecule.

Tables

Table 1. Crystallographic data and structure refinement of DCMSP.

Table 2. Hydrogen bond geometry (°, Å) in the DCMSP.

Table 3. Simulated wavenumbers (scaled), experimental IR, Raman bands and assignments for DCMSP.

Table 4. Theoretical electronic absorption spectra of title compound (absorption wavelength λ (nm), excitation energies E (eV) and oscillator strengths (*f*)) using TD-DFT/ B3LYP/ 6311++G(d,p) method.

Table 5. Second-order perturbation theory analysis of Fock matrix in NBO basis corresponding to the intramolecular bonds of the title compound.

Table 6. NBO results showing the formation of Lewis and non-Lewis orbitals.

Table 7. The values of the dipole moment (in D) and the linear polarizability (in 10^{-24} esu) were calculated using $\mathrm{MP2/6-311++G(d,p)}$ and for values of the second hyperpolarizability in (in 10^{-36} esu) we used $\mathrm{CAM-B3LYP/6-311++G(d,p)}$ for DCMSP embedded molecule in the case static.

Table 8. The values of the linear polarizability (in 10^{-24} esu) were calculated $\mathrm{CAM-B3LYP/6-311++G(d,p)}$ and for values of the second hyperpolarizability in (in 10^{-36} esu) we used $\mathrm{CAM-B3LYP/6-311++G(d,p)}$ for DCMSP embedded molecule (ω in a.u.).

Table 9. DFT/CAM-B3LYP/ 6-311++G(d,p) results for the linear refractive index and third-order nonlinear susceptibility ($10^{-22}\,\mathrm{m^2/V^2}$) for the case dynamic (ω = 0.085 a.u.) of the DCMSP crystal.

Table 1.

Crystallographic data and structure refinement of DCMSP.

Formula	C5 H4 Cl2 N2 O2 S
Formula Weight	227.06
Crystal System	triclinic
Space group	$P\bar{1}$
a, b, c [Å]	7.9208(4) 8.6194(5) 14.3769(8)
α, β, γ [°]	85.404(3) 88.336(3) 63.205(3)
V [$Å^3$]	873.31(9)
Z	4
ρ_{calcd} [g/cm^3]	1.727
μ [/mm]	0.940
F(000)	456
Crystal Size [mm]	0.12 x 0.16 x 0.18
Temperature (K)	296
λ [Å]	0.71073
Theta Min-Max [°]	2.8, 29.1
Index ranges	$-10 \leq h \leq 10$ $-11 \leq k \leq 11$ $-19 \leq l \leq 19$
Rflns.Total.	16835
Unique rflns	4645
R_{int}	0.029
Observed Data [I > 2.0 sigma(I)]	3895
N_{ref}, N_{par}	4677, 258
R	0.0414
wR_2	0.1173
Max. and Av. Shift/Error	0.00, 0.00
Min. and Max. Resd. Dens. [e/ $Å^3$]	-0.53, 0.70

Table 2.
Hydrogen bond geometry (°, Å) in the DCMSP

A−H···B	A−H (Å)	H···B (Å)	A−H···B (Å)	A−H···B (°)
C4−H13···O10	0.93	2.29	3.201(3)	166
C12−H14···O11	0.96	2.40	3.216(7)	143

Table 3
Simulated wavenumbers (scaled), experimental IR, Raman bands and assignments for DCMSP.

B3LYP/6-311++G(d,p)			ν(IR) (cm^{-1})	ν(Raman) (cm^{-1})	Assignment (%)
Scaled (cm^{-1})	IR activity	Raman activity			
3114	4.6075	77.7954	3101	3101	νCH(100)
3064	3.00E-04	34.2458	3058	3060	$\nu_{asy}CH_3$(50)
3043	0.023	70.6943	-	-	$\nu_{asy}CH_3$(54) $\nu_{asy}CH_3$(23)
2949	0.2021	161.083	-	2946	$\nu_{sy}CH_3$(46) $\nu_{sy}CH_3$(27)
1509	385.678	7.9379	1512	1511	νCN(13) νCC(39)
1499	313.329	17.2595	-	-	νCN(33)
1395	13.0804	2.966	1400	1399	$\delta_{asy}CH_3$(53) $\delta_{asy}CH_3$(11) γHCSC(11)
1392	7.4147	7.5257	-	-	$\delta_{asy}CH_3$(36) $\delta_{asy}CH_3$(17) γHCSC(17)
1356	105.52	1.0988	1363	1357	νCN(19) δCHI(35)
1301	11.3561	1.3296	1297	1298	$\delta_{sy}CH_3$(32) $\delta_{sy}CH_3$(27)
1267	105.715	2.4962	1255	1258	δNCN(26) νCN(22) νCC(12)
1245	223.053	12.3783	1250	1246	$\nu_{as}SO_2$ (48)
1201	10.3479	5.7275	1198	1214	νCN(39) νCC(15)
1176	101.403	3.4799	-	1174	δNCN(20) δCNC(20)
1084	107.469	1.6009	1082	1083	δCHI(52) δCCN(13) νCC(10)
1063	142.063	32.5791	-	1066	ν_sSO_2 (42)
963	6.6406	36.646	970	972	δNCN(10)
948	29.7999	2.0631	-	946	δCH_3(16) γHCSC(30)
941	0.3273	2.3708	-	941	δCH_3(14) γHCSC(39) γHCSC(13)

836	16.878	0.0838	-	835	γHCPh(77)
804	18.7522	0.5473	800	802	νSC(20) νClC(25)
789	145.096	0.0477	-	-	νClC(30) νClC(10)
748	0.0523	0.0022	743	741	τNCNC(16) τCNCN(24)
694	107.481	15.2176	692	694	νSC(65)
605	0.0016	0.5517	612	611	γCHI(10) γOCCS(12)
582	0.0044	0.0426	-	585	γClCNC(34)
502	96.1014	3.274	-	503	νSC(10) δSO_2scissoring (11), γOCOS(47)
484	10.5672	4.2465	-	501	νSC(13) δCCl(11), δSO_2wagging(29)
420	17.802	4.0764	-	420	δCSC(10) νClC(22) νClC(18) δSO_2twisting (17)
413	6.2385	0.6764	-	-	δCCl(22) δSO_2(26)
398	12.0064	8.0636	-	383	νClC(27) νClC(25)
324	3.3673	1.4614	-	-	δOSC(23) γOCCS(54)
268	0.4623	9.2941	-	272	OCOC(11) δSO_2rocking (11)
253	3.3337	0.5337	-	253	δOSC(11) δOSC(56) γOCCS(10)
239	4.9607	4.2871	-	223	δCSC(66)
190	0.0398	0.0849	-	192	τCH3(24) γHCSC(29)
188	0	0.0735	-	-	γHCSC(24) γCCl(15)
173	0.0156	4.2074	-	163	δClCN(35)
139	2.427	0.9527	-	129	γCCl(12)
87	0.0108	1.7198	-	75	γOCCS(15)
17	5.3392	0.4828	-	-	δCSCN(93)

[a] υ-stretching; δ-in-plane deformation; γ-out-plane deformation; τ-torsion; potential energy distribution is given in brackets (%) in the assignment column.

Table 4.

Theoretical electronic absorption spectra of title compound (absorption wavelength λ (nm), excitation energies E (eV) and oscillator strengths (*f*)) using TD-DFT/B3LYP/6311++G(d,p) method.

Excitation	CI expansion	Energy Coefficient (eV)	Wavelength (nm)		Oscillator strength (*f*)
			Exp	Cal	
57→58 57→59	0.48623 0.11512	4.7920	-	258	0.0001
57→58 57→59	0.66503 0.12695	4.8509	-	255	0.0020
54→58 54→59 57→58 57→59	0.43198 0.10290 0.35235 0.41668	4.9013	254	253	0.0041

Table 5.
Second-order perturbation theory analysis of Fock matrix in NBO basis corresponding to the intramolecular bonds of the title compound.

Donor(i)	Type	ED/e	Acceptor(j)	Type	ED/e	E(2)[a]	E(j)-E(i)[b]	F(i,j)[c]
N2-C1	σ	1.98039	N2-C3	σ*	0.03521	1.66	1.38	0.043
			N6-C1	σ*	0.03712	1.49	1.40	0.041
			C3-Cl7	σ*	0.05322	5.04	1.02	0.065
N2-C3	σ	1.98280	N2-C1	σ*	0.04159	1.68	1.40	0.044
			C1-S9	σ*	0.25941	3.21	1.00	0.054
			C3-C4	σ*	0.03767	1.90	1.41	0.046
N6-C5	σ	1.98349	N6-C1	σ*	0.03712	1.67	1.40	0.043
			C1-S9	σ*	0.25941	3.12	1.00	0.053
			C4-C5	σ*	0.03892	1.82	1.40	0.045
C1-S9	σ	1.96144	N2-C3	σ*	0.03521	3.67	1.15	0.058
			N6-C5	σ*	0.03320	3.68	1.16	0.058
			C1-S9	σ*	0.25941	0.99	0.76	0.026
			C12-S9	σ*	0.17263	1.65	0.79	0.033
			O11-S9	σ*	0.13908	2.70	0.95	0.047
			O10-S9	σ*	0.13907	2.70	0.95	0.047
C3-C4	σ	1.97826	N2-C3	σ*	0.03521	2.04	1.26	0.045
			C4-C5	σ*	0.03892	2.71	1.28	0.053
			C5-Cl8	σ*	0.05459	4.62	0.90	0.058
C3-Cl7	σ	1.98578	N2-C1	σ*	0.04159	3.06	1.24	0.045
			C4-C5	σ*	0.03892	1.99	1.25	0.045
C4-C5	σ	1.97774	N6-C5	σ*	0.03320	1.94	1.27	0.044
			C3-C4	σ*	0.03767	2.75	1.28	0.053
			C3-Cl7	σ*	0.05322	4.88	0.89	0.059
C5-Cl8	σ	1.98587	N6-C1	σ*	0.03712	3.03	1.24	0.055
			C3-C4	σ*	0.03767	1.96	1.26	0.045
C12-S9	σ	1.97700	O11-S9	σ*	0.13908	2.62	0.96	0.046
				σ*	0.13907	2.62	0.96	0.046
O11-S9	σ	1.98745	N2-C1	σ*	0.04159	0.56	1.47	0.026
			C1-S9	σ*	0.25941	1.16	1.07	0.034
			O11-S9	σ*	0.13908	0.62	1.26	0.026
			O10-S9	σ*	0.13907	1.33	1.26	0.038
O10-S9	σ	1.98745	N2-C1	σ*	0.04159	0.56	1.47	0.026
			C1-S9	σ*	0.25941	1.16	1.07	0.034
			O11-S9	σ*	0.13908	1.33	1.26	0.038
			O10-S9	σ*	0.13907	0.62	1.26	0.026
LP N2	σ	1.88970	N6-C1	σ*	0.03712	12.49	0.89	0.096
	-		C1-S9	σ*	0.25941	4.80	0.48	0.045
	-		C3-C4	σ*	0.03767	9.87	0.90	0.086
	-		C3-Cl7	σ*	0.05322	4.20	0.51	0.042
LP N6	σ	1.88473	N2-C1	σ*	0.04159	13.01	0.87	0.097
	-		C1-S9	σ*	0.25941	4.53	0.47	0.043
	-		C4-C5	σ*	0.03892	10.25	0.88	0.086
	-		C5-Cl8	σ*	0.05459	4.51	0.050	0.043
LP O11	σ	1.98470	C12-S9	σ*	0.17263	0.74	0.94	0.025
	-		O10-S9	σ*	0.13907	1.51	0.10	0.038
LP O11	π	1.81229	C1-S9	σ*	0.25941	8.33	0.38	0.051

	-		C12-S9	σ*	0.17263	17.58	0.41	0.076
	-		O10-S9	σ*	0.13907	3.34	0.57	0.040
LP O10	σ	1.98470	C12-S9	σ*	0.17263	0.74	0.94	0.025
	-		O11-S9	σ*	0.13908	1.51	1.10	0.038
LP O10	π	1.81229	C1-S9	σ*	0.25941	8.34	0.38	0.051
	-		C12-S9	σ*	0.17263	17.58	0.41	0.076
	-		O11-S9	σ*	0.13908	3.34	0.57	0.040
LP Cl7	σ	1.99207	N2-C3	σ*	0.03521	1.08	1.43	0.035
	-		C3-C4	σ*	0.03767	1.77	1.46	0.046
LP Cl7	π	1.96416	N2-C3	σ*	0.03521	6.73	0.82	0.066
	-		C3-C4	σ*	0.03767	3.89	0.85	0.051
LP Cl8	σ	1.99205	N6-C5	σ*	0.03320	1.05	1.44	0.035
	-		C4-C5	σ*	0.03892	1.75	1.45	0.045
LPCl8	π	1.96372	N6-C5	σ*	0.03320	6.75	0.83	0.067
	-		C4-C5	σ*	0.03892	3.95	0.84	0.051

[a] E(2) means energy of hyper-conjugative interactions (stabilization energy in kJ/mol)
[b] Energy difference (a.u) between donor and acceptor i and j NBO orbitals
[c] F(i,j) is the Fock matrix elements (a.u) between i and j NBO orbitals

Table 6.

NBO results showing the formation of Lewis and non-Lewis orbitals.

Bond(A-B)	ED/e[a]	EDA%	EDB%	NBO	s%	p%
σ N2-C1	1.98039	60.01	39.99	0.7746($sp^{1.80}$)N+	35.61	64.21
-	-0.92615	-	-	0.6324($sp^{1.63}$)C	38.04	61.91
σ N2-C3	1.98280	59.38	40.62	0.7706($sp^{1.74}$)N+	36.04	63.41
-	-0.92469	-	-	0.6373($sp^{1.97}$)C	33.64	66.31
σ N6-C5	1.98349	59.25	40.75	0.7698($sp^{1.74}$)N+	36.43	63.39
-	-0.92487	-	-	0.6383($sp^{1.96}$)C	33.82	66.13
σ C1-S9	1.96144	52.78	47.22	0.7265($sp^{3.09}$)C+	24.41	75.51
-	-0.68830	-	-	0.6872($sp^{3.72}$)C	20.86	77.68
σ C3-C4	1.97826	49.77	50.23	0.7055($sp^{1.39}$)C+	41.83	58.15
-	-0.80294	-	-	0.7087($SP^{1.92}$)C	34.17	65.71
σ C3-Cl7	1.98578	46.82	53.18	0.6842($sp^{3.09}$)C+	24.37	75.42
-	-0.77280	-	-	0.7293($sp^{4.96}$)C	16.70	82.77
σ C4-C5	1.97774	50.30	49.70	0.7092($sp^{1.94}$)C+	33.98	65.90
-	-0.79785	-	-	0.7050($sp^{1.41}$)C	41.48	58.50
σ C5-C18	1.98587	46.99	53.01	0.6855($sp^{3.07}$)C+	24.52	75.27
-	-0.77008	-	-	0.7281($sp^{4.96}$)C	16.70	82.77
σ C12-S9	1.97700	49.39	50.61	0.7028($sp^{4.06}$)C+	19.74	80.16
-	-0.69720	-	-	0.7114($sp^{3.01}$)S	24.61	74.11
σ O11-S9	1.98745	63.60	36.40	0.7975($sp^{3.30}$)O+	23.24	76.62
	-0.99768			0.6035($sp^{2.59}$)S	27.45	71.04
σ O10-S9	1.98745	63.60	36.40	0.7975($sp^{3.30}$)O+	23.24	76.62
	-0.99770			0.6035($sp^{2.59}$)S	27.45	71.04
σ LP N2	1.88970	-	-	$sp^{2.57}$	27.94	71.89
-	-0.41198	-	-	-	-	-
σ LP N6	1.88473	-	-	$sp^{2.58}$	27.87	71.95
-	-0.40010	-	-	-	-	-
σ LP O11	1.98470	-	-	$sp^{0.30}$	76.72	23.27
-	-0.83778	-	-	-	-	-
π LP O11	1.81229	-	-	$sp^{99.99}$	0.07	99.85
-	-0.30745	-	-	-	-	-
σ LP O10	1.98470	-	-	$sp^{0.30}$	76.72	23.27
-	-0.83778	-	-	-	-	-
π LP O10	1.81229	-	-	$sp^{99.99}$	0.07	99.85
	-0.30745	-	-	-	-	-
σ LP Cl7	1.99207	-	-	$sp^{0.20}$	83.30	16.69
	-0.97653	-	-	-	-	-
π LP Cl7	1.96416	-	-	$sp^{99.99}$	0.10	99.87
	-0.36173	-	-	-	-	-
σ LP Cl8	1.99205	-	-	$sp^{0.20}$	83.31	16.67
	-0.97109	-	-	-	-	-
π LP Cl8	1.96372	-	-	$sp^{99.99}$	0.10	99.97
	-0.35618	-	-	-	-	-

[a] ED/e is expressed in a.u.

Table 7.

The values of the dipole moment (in D) and the linear polarizability (in 10^{-24} esu) were calculated using $MP2/6-311++G(d,p)$ and for values of the second hyperpolarizability in (in 10^{-36} esu) we used $CAM-B3LYP/6-311++G(d,p)$ for DCMSP embedded molecule in the case static.

μ_x	μ_y	μ_z	μ			
1.05	5.17	2.17	5.71			
α_{xx}	α_{xy}	α_{yy}	α_{xz}	α_{yz}	α_{zz}	$\bar{\alpha}$
16.58	2.72	17.36	3.11	-2.71	18.08	17.34
γ_{xxxx}	γ_{yyyy}	γ_{zzzz}	γ_{xxyy}	γ_{yyzz}	γ_{xxzz}	$\bar{\gamma}$
10.90	8.52	10.12	3.64	3.45	4.53	10.55

Table 8:
The values of the linear polarizability (in 10^{-24} esu) were calculated $CAM-B3LYP/6-311++G(d,p)$ and for values of the second hyperpolarizability in (in 10^{-36} esu) we used $CAM-B3LYP/6-311++G(d,p)$ for DCMSP embedded molecule ($\omega\ in\ a.u.$).

Frequency (ω)	$\langle\alpha(-\omega,\omega)\rangle$	$\langle\gamma(-\omega;\omega,0,0)\rangle$	$\langle\gamma(-\omega;\omega,\omega,-\omega)\rangle$
0.000	17.31	10.55	10.55
0.002	17.31	10.62	10.68
0.004	17.32	10.62	10.69
0.006	17.32	10.63	10.70
0.008	17.32	10.64	10.72
0.010	17.32	10.65	10.74
0.024	17.37	10.79	11.03
0.043	17.51	11.20	11.84
0.050	17.58	11.42	12.29
0.060	17.70	11.81	13.07
0.070	17.85	12.30	14.05
0.072	17.89	12.42	14.28
0.080	18.03	12.92	15.29
0.086	18.14	13.29	16.03
0.090	18.25	13.70	16.84
0.100	18.50	14.67	18.78

Table 9:
DFT/CAM-B3LYP/ 6-311++G(d,p) results for the linear refractive index and third-order nonlinear susceptibility (10^{-22} m^2/V^2) for the case dynamic (ω = 0.085 a.u.) of the DCMSP crystal.

Sample	$n_0(\omega)$	$\chi^{(3)}(-\omega;\omega,\omega,-\omega)$
DCMSP (present work)	1.613	56.74
(2E)-1-(4-bromophenyl)-3-[4-methylsulfanyl) phenyl]prop-2-en-1-one (4Br4MSP) [14]	1.363	2.30
(2E)-1-(3-bromophenyl)-3-[4(methylsulfanyl) phenyl]prop-2-en-1-one (3Br4MSP) [14]	1.365	1.99
(2E)-3[4(methylsulfanyl)phenyl]-1-(4-nitrophenyl)prop-2-en-1-one (4N4MSP) [14]	1.360	2.37

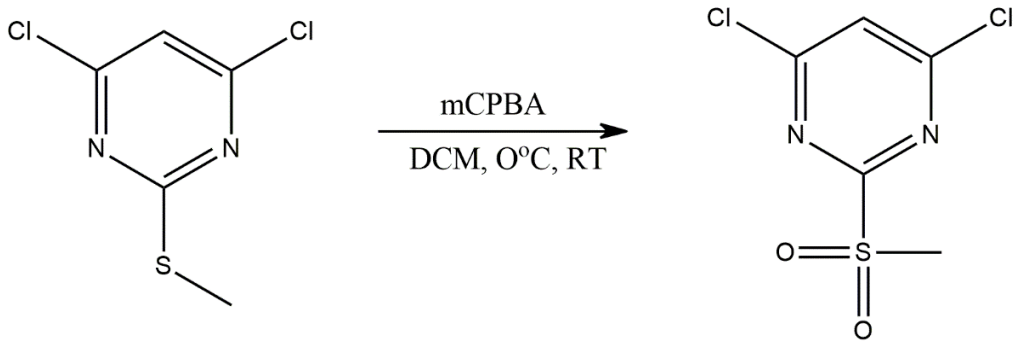

Scheme -1: Synthetic scheme for 4,6-dichloro-2-(methylsulfonyl)pyrimidine

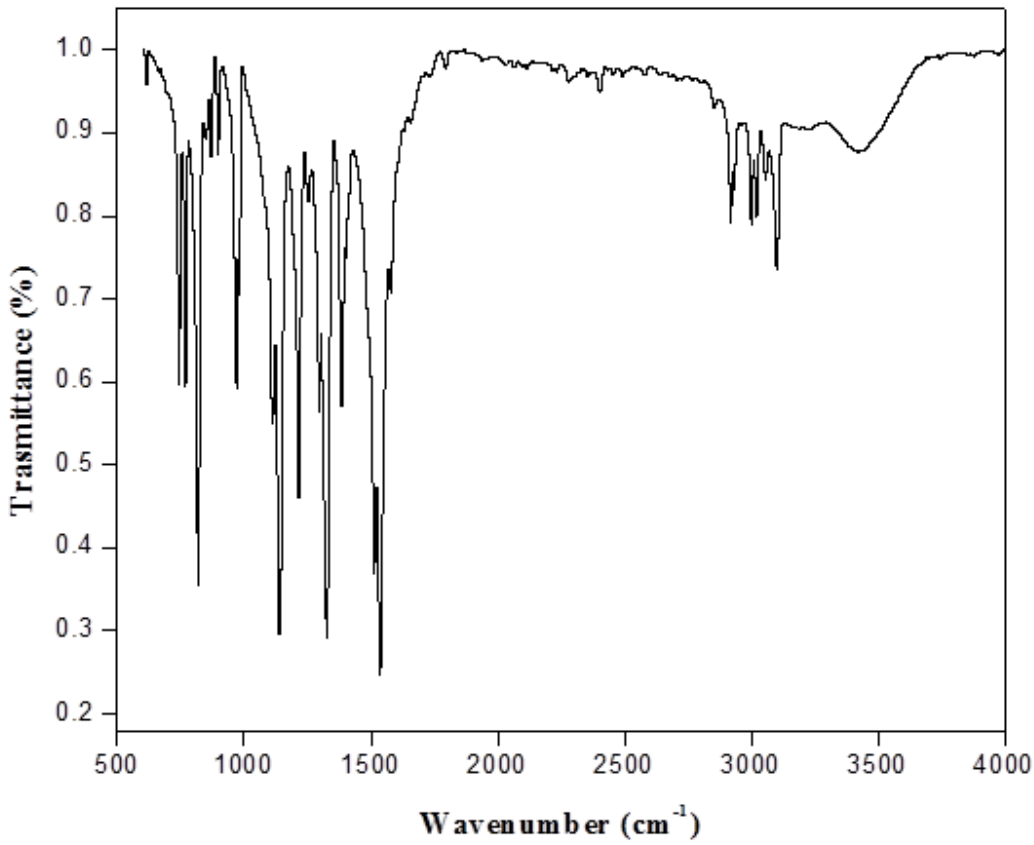

Figure 1. Fourier Transform Infra-Red spectrum of DCMSP.

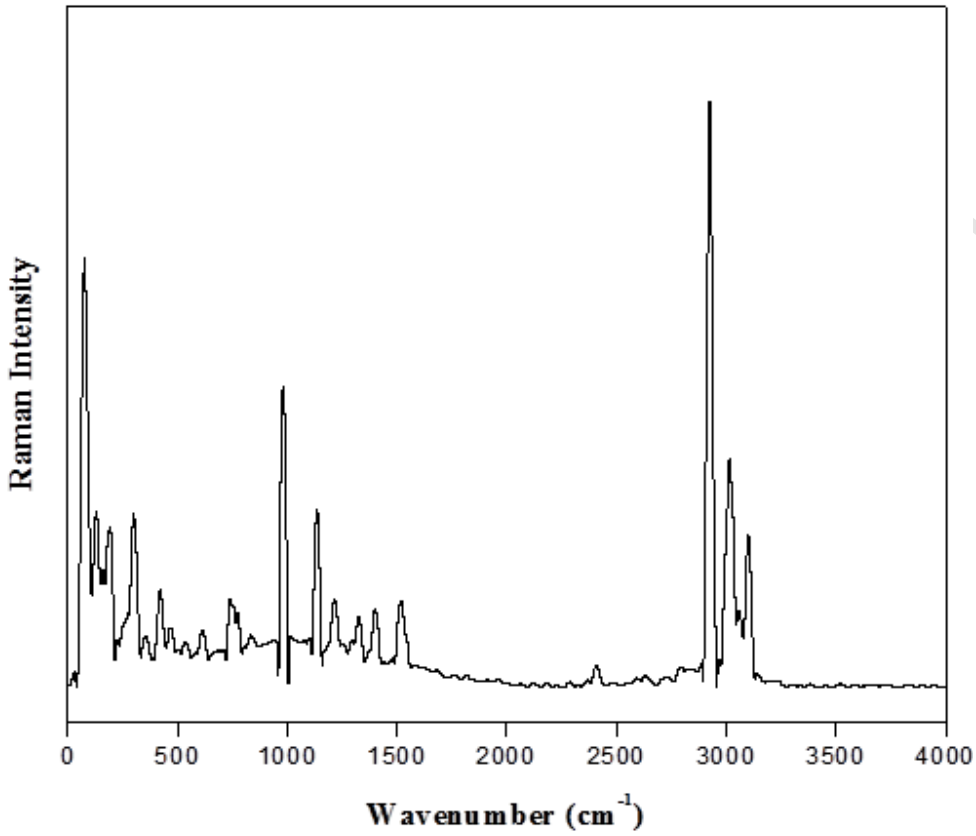

Figure 2. Fourier Transform Raman spectrum of DCMSP.

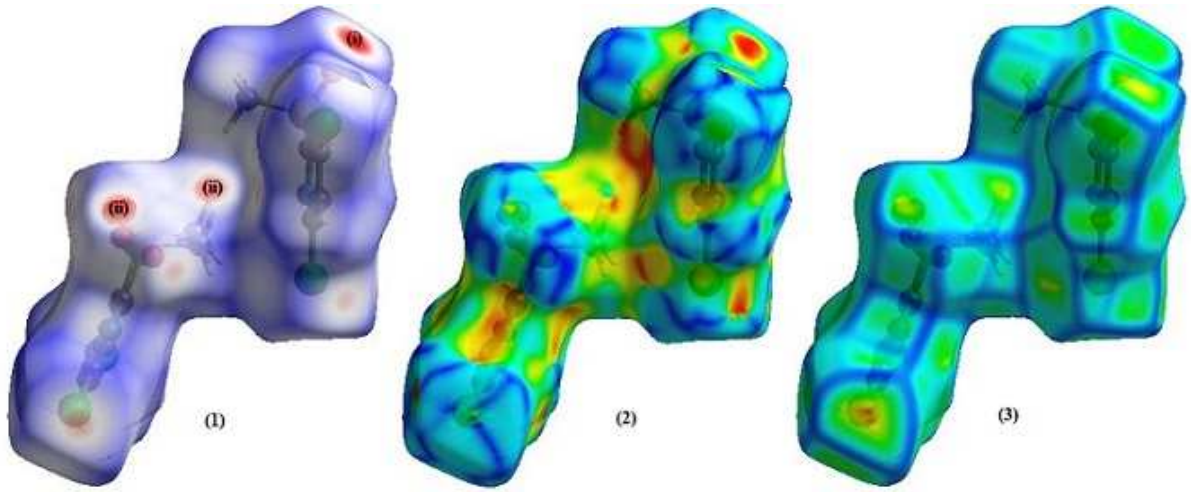

(A) Hirshfeld surfaces of DCMSP d_{norm} -0.356 (red) to 1.191 Å au (blue) (1), *shape index* -1.0 (concave) to 1.0 Å au (convex) (2) and *curvedness* (3) -4.0 (flat) to 0.4 Å au (singular). The d_{norm} mapped surface exhibit two interactions; the first interaction between the oxygen atom of the sulfonyl group (S=O) and with the hydrogen atom of pyrimidine ring, which can be visualized as bright red spot and labelled as (i). The second interaction between the oxygen atom of sulfonyl group (S=O) and with the hydrogen atom of a methyl group (CH_3), which can be visualized as bright red spots and labelled as (ii).

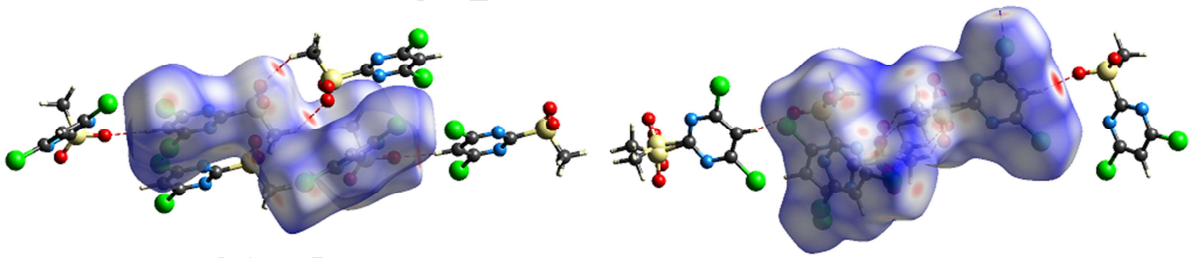

(B) View of C-H···O contacts on d_{norm} surface of DCMSP.

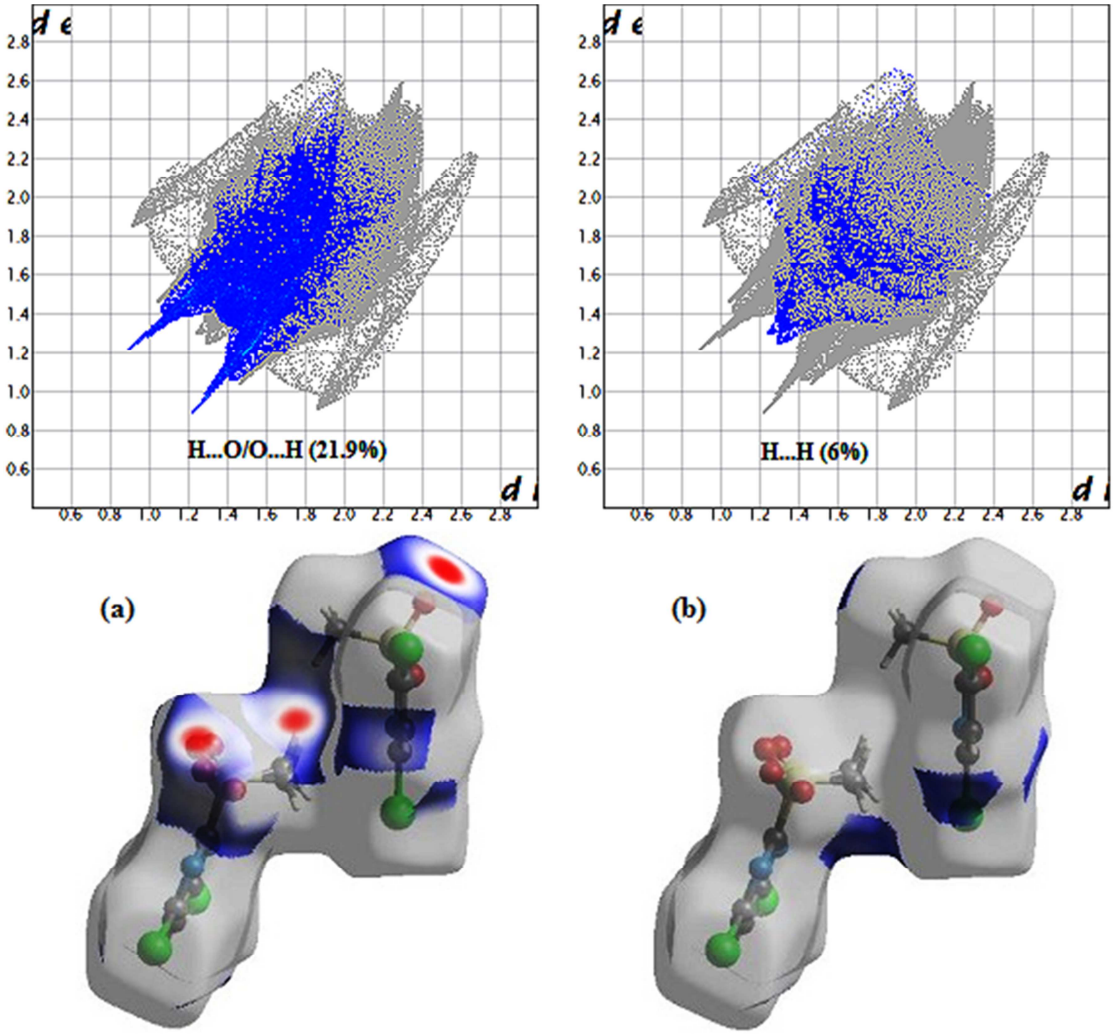

(C) 2D Fingerprint plots of the DCMSP compound and various interactions are visualized with percentage of contact (a) O···H/H···H (21.9%)and (c) H···H (6%) interactions. Here d_i is the closest internal distance from a given point on the Hirshfeld surface and d_e is the closest external contacts.

Figure 3. Analysis of 3D-Hirshfeld surface and 2D-Finger print plots of DCMSP.

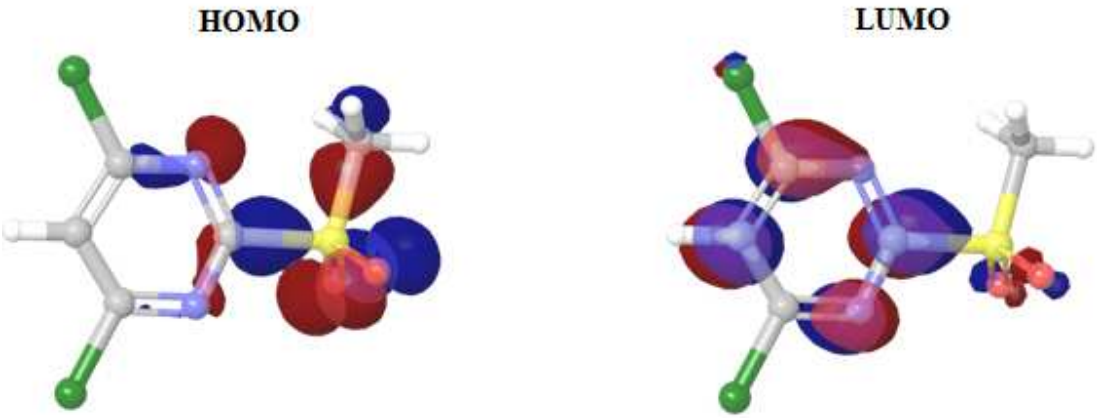

Figure 4. HOMO-LUMO plots of DCMSP.

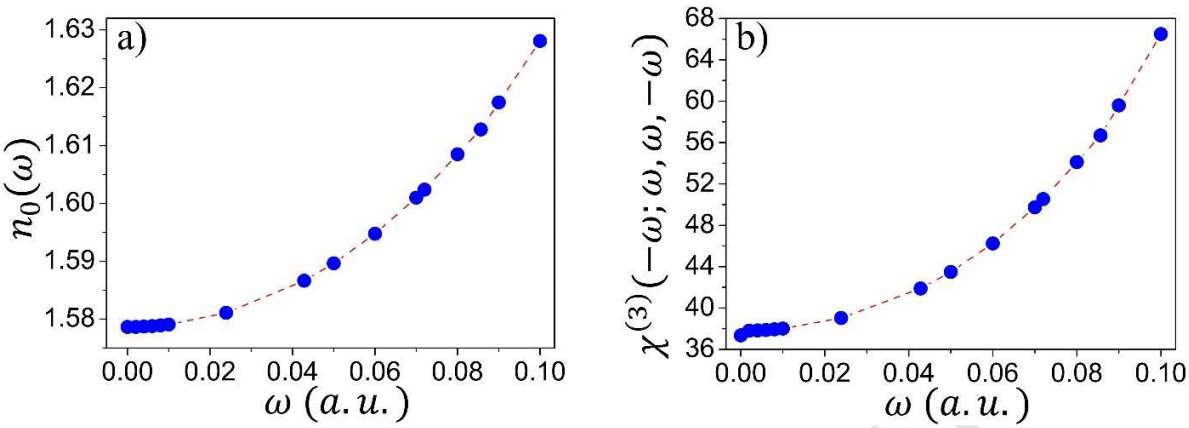

Figure 5. Dynamic evolution of the studied values (a) of the linear refractive index and (b) third-order nonlinear optical susceptibility $\chi^{(3)}$ (in $10^{-22}\ \mathrm{m}^2/\mathrm{V}^2$) of the DCMSP crystal with respective values of frequencies.

.

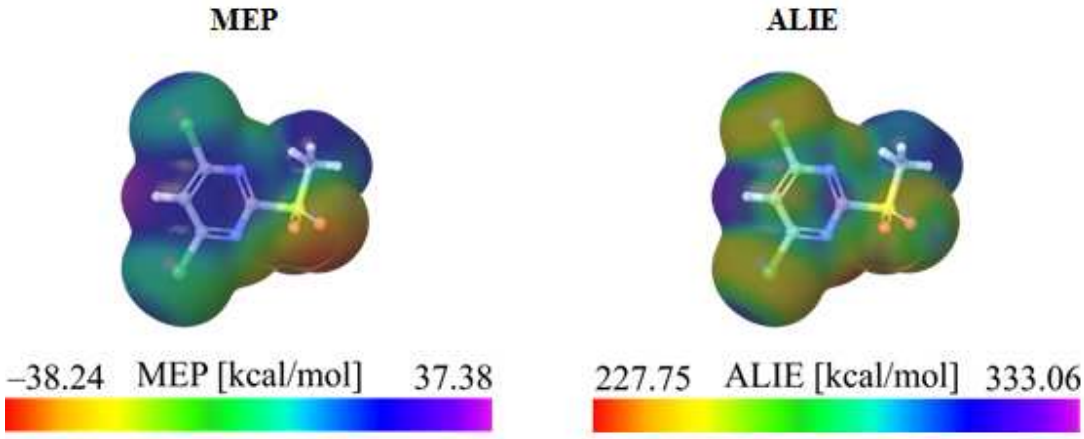

Figure 6. MEP and ALIE surfaces of DCMSP molecule

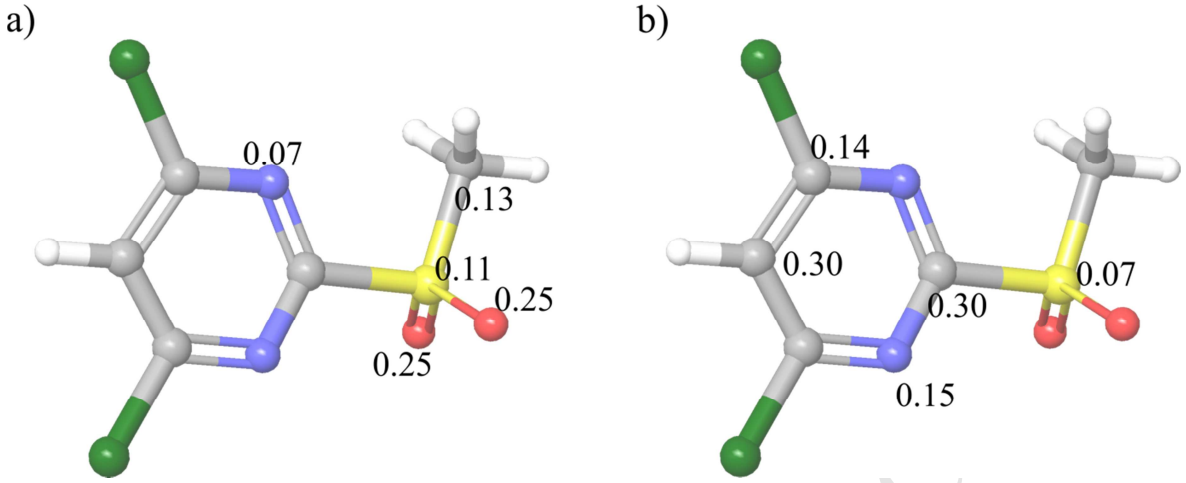

Figure 7. Fukui indices for DCMSP molecule a) f_{NN}^{HOMO} and b) f_{NN}^{LUMO} indices

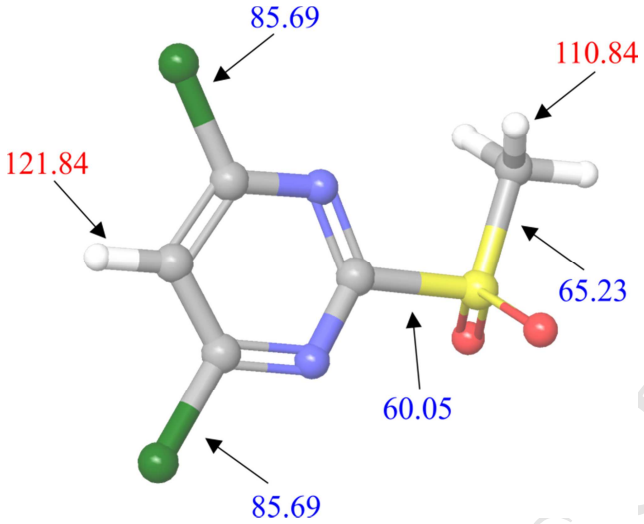

Figure 8. H-BDE (red color) and BDE (blue color) values for DCMSP molecule.

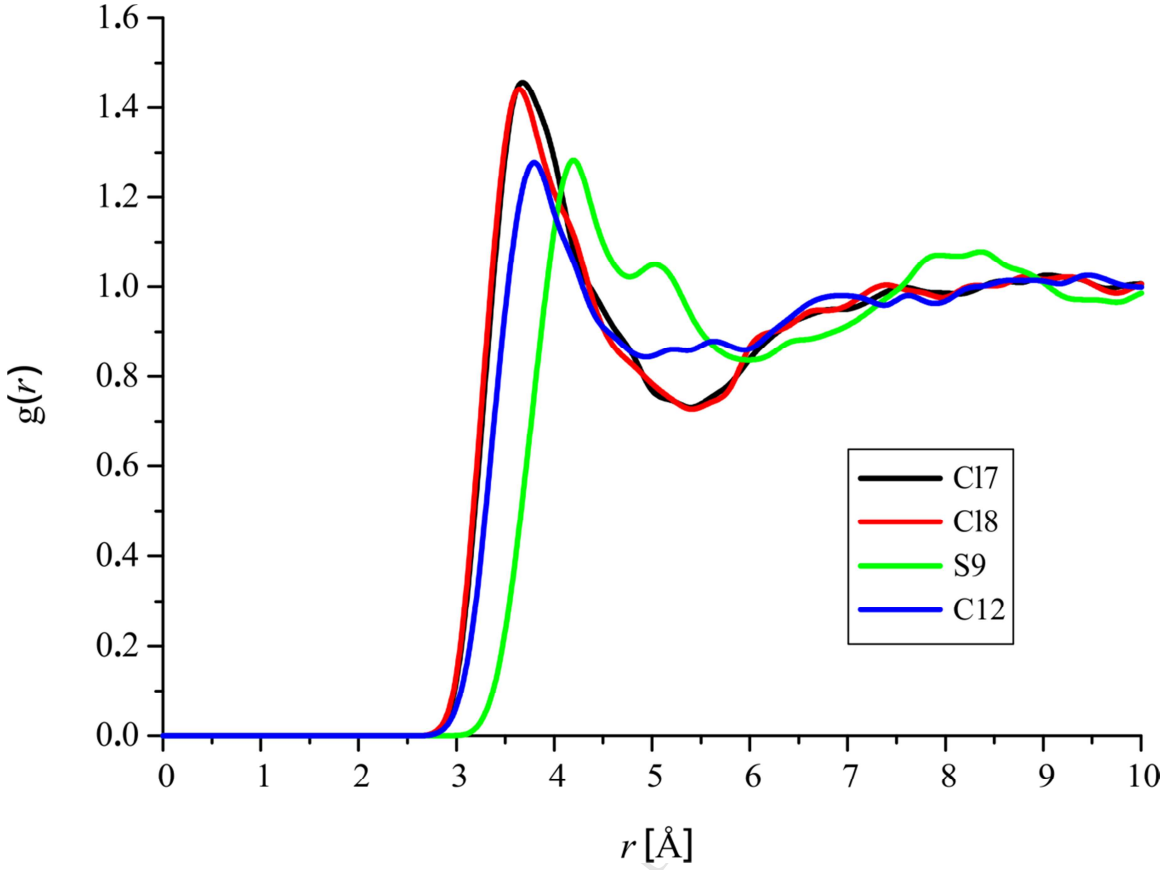

Figure 9. Representative RDFs of DCMSP molecule.

Highlights

- Most reactive sites are identified by using MEP and ALIE plots.
- Autoxidation and degradation properties are investigated from BDE and RDF calculations.
- DCMSP crystal exhibit potential candidate for application in nonlinear optical devices.
- A detailed interpretation of FT-IR and FT-Raman spectra of DCMSP reported.